Chloride Channels of Glycine and GABA Receptors with Blockers: Monte Carlo Minimization and Structure-Activity Relationships

Boris S. Zhorov*† and Piotr D. Bregestovski*

*INSERM U-261 Neurobiologie Cellulaire, Institut Pasteur, Paris, France; and †Sechenov Institute of Evolutionary Physiology and Biochemistry of the Russian Academy of Sciences, St. Petersburg, Russia

ABSTRACT GABA and glycine receptors (GlyRs) are pentameric ligand-gated ion channels that respond to the inhibitory neurotransmitters by opening a chloride-selective central pore lined with five M2 segments homologous to those of α_1 GlyR/ARVG$^{2'}$LGIT$^{6'}$TVLTMTTQSSGSR. The activity of cyanotriphenylborate (CTB) and picrotoxinin (PTX), the best-studied blockers of the Cl^- pores, depends essentially on the subunit composition of the receptors, in particular, on residues in positions 2′ and 6′ that form the pore-facing rings R$^{2'}$ and R$^{6'}$. Thus, CTB blocks α_1 and α_1/β, but not α_2 GlyRs (Rundström, N., V. Schmieden, H. Betz, J. Bormann, and D. Langosch. 1994. *Proc. Natl. Acad. Sci. U.S.A.* 91:8950–8954). PTX blocks homomeric receptors (α_1 GlyR and rat ρ_1 GABAR), but weakly antagonizes heteromeric receptors (α_1/β GlyR and ρ_1/ρ_2 GABAR) (Pribilla, I., T. Takagi, D. Langosch, J. Bormann, and H. Betz. 1992. *EMBO J.* 11:4305–4311; Zhang D., Z. H. Pan, X. Zhang, A. D. Brideau, and S. A. Lipton. 1995. *Proc. Natl. Acad. Sci. U.S.A.* 92:11756–11760). Using as a template the kinked-helices model of the nicotinic acetylcholine receptor in the open state (Tikhonov, D. B., and B. S. Zhorov. 1998. *Biophys. J*. 74:242–255), we have built homology models of GlyRs and GABARs and calculated Monte Carlo-minimized energy profiles for the blockers pulled through the pore. The profiles have shallow minima at the wide extracellular half of the pore, a barrier at ring R$^{6'}$, and a deep minimum between rings R$^{6'}$ and R$^{2'}$ where the blockers interact with five M2s simultaneously. The star-like CTB swings necessarily on its way through ring R$^{6'}$ and its activity inversely correlates with the barrier at R$^{6'}$: Thr$^{6'}$s and Ala$^{2'}$s in α_2 GlyR confine the swinging by increasing the barrier, while Gly$^{2'}$s in α_1 GlyR and Phe$^{6'}$s in β GlyR shrink the barrier. PTX has an egg-like shape with an isopropenyl group at the elongated end and the rounded end trimmed by ether and carbonyl oxygens. In the optimal binding mode to α_1 GlyR and ρ_1 GABAR, the rounded end of PTX accepts several H-bonds from Thr$^{6'}$s, while the elongated end enters ring R$^{2'}$. The lack of H-bond donors on the side chains of Phe$^{6'}$s (β GlyR) and Met$^{6'}$s (ρ_2 GABAR) deteriorates the binding. The hydrophilic elongated end of picrotin does not fit the hydrophobic ring of Pro$^{2'}$s/Ala$^{2'}$s in GABARs, but fit a more hydrophilic ring with Gly$^{2'}$s in GlyRs. This analysis provides explanations for structure-activity relationships of noncompetitive agonists and predicts a narrow pore of LGICs in agreement with experimental data on the permeation of organic cations.

INTRODUCTION

The inhibitory GlyR and $GABA_A$ (GABAR) belong to the family of LGICs, which also comprise excitatory nAChR and 5-hydroxytryptamine (5-HT3) receptors, as well as the inhibitory glutamate receptors (Betz, 1990; Ortells and Lunt, 1995; Cleland, 1996). LGICs are pentameric proteins, each subunit having a large extracellular domain at the N-end, four transmembrane segments (M1-M4), and an intracellular (M3-M4) loop. Although the folding of LGIC proteins remains unknown, there is a consensus that five M2s, predominantly in the α-helical conformation, contribute to the central pore (Changeux et al., 1992; Galzi and Changeux, 1995; Karlin and Akabas, 1995). M2s are, probably, kinked in their middle part (Unwin, 1995). The five-helical bundle of nAChR is believed to have a funnel-like shape with a narrow cytoplasmic end and several rings of homologous residues facing the pore (Changeux et al., 1992). The residues in the rings were demonstrated to govern ion conductance (Imoto et al., 1988), ion selectivity (Galzi et al., 1992), gating (Labarca et al., 1995), desensitization (Revah et al., 1991), and pharmacological properties (reviewed by Arias, 1998) of LGICs.

The central pore of LGICs is the only functional domain for which structure-function relationships are relatively well understood due to numerous electrophysiological, pharmacological, mutagenesis, and molecular modeling studies. Data on permeability of organic cations via nAChRs suggest the minimal profile of the open pore as a square of 6.5 × 6.5 Å (Dwyer et al., 1980) or a circle of 7.6 Å diameter (Nutter and Adams, 1995). Analogous approaches predict the minimal circular profiles of the open pore to have a diameter of 5.2–5.4 Å in GlyR (Bormann et al., 1987; Rundström et al., 1994), 5.6 Å in GABAR (Bormann et al., 1987), and 7.6 Å in the 5-HT3 receptor (Yang, 1990). The analysis of the conformation-activity relationships of noncompetitive pentamethylenebisammonium antagonists of nAChR (Zhorov et al., 1991; Brovtsyna et al., 1996) predicted the pore profiles at the levels of the two ammonium groups as rectangles of 6.1 × 8.3 Å and 5.5 × 6.4 Å.

Received for publication 29 July 1999 and in final form 9 November 1999.

Address reprint requests to Dr. Boris Zhorov, Dept. of Biochemistry, McMaster University, 1200 Main Street West, Hamilton, Ontario L8N 3Z5, Canada. Tel.: 905-525-9140 ext 22864; Fax: 905-522-9033; E-mail: zhorov@fhs.mcmaster.ca.

Abbreviations used: GlyR, glycine receptor; AChR, acetylcholine receptor; CTB, cyanotriphenylborate; GABAR, GABA receptor; LGIC, ligand-gated ion channels; MCM, Monte Carlo minimization; MEC, minimum-energy conformer; PTN, picrotin; PTX, picrotoxinin.

0006-3495/00/04/1786/18 $2.00

However, the low-resolution electron cryomicroscopy images of the nicotinic acetylcholine receptor in the open state imply a wider central pore (Unwin, 1995). The controversial data on the dimensions of the pore are reflected in recent structural models of the nAChR with M2s either tightly packed at the cytoplasmic half (Ortells and Lunt, 1996; Tikhonov and Zhorov, 1998) or distant from each other (Sankararamakrishnan et al., 1996; Adcock et al., 1998).

A knowledge of the pore architecture in LGICs is necessary for understanding functions of the pore-lining residues and mechanisms of the channel block by noncompetitive antagonists. A touchstone for structural models of the pore is their ability to explain structure-activity relationships of ligands. The pore region of nAChRs comprises binding sites for numerous noncompetitive antagonists (Arias, 1998). In contrast, little is known about the mechanisms of the block of ligand-gated Cl^- channels. CTB (see Fig. 1) inhibits GlyRs by a noncompetitive, channel-blocking mechanism (Rundström et al., 1994). PTX (Fig. 1) is the antagonist of GlyRs (Pribilla et al., 1992; Lynch et al., 1995), GABARs (Hosie et al., 1997; Zhang et al., 1995a), as well as of the inhibitory glutamate receptor (Cleland, 1996). All these receptors activate Cl^--selective channels.

The interpretations of experimental results on PTX action are obscured by the fact that, unlike the case of the negatively charged CTB, which is expected to enter a Cl^- channel, the energy contributions that stabilize the electrically neutral PTX in the anionic pore remain unknown. Two main mechanisms of PTX action have been proposed. Pribilla et al. (1992) interpreted results of their mutagenesis, electrophysiological, and ligand-binding studies of GlyRs in favor of a noncompetitive mechanism of PTX block. Using a similar approach, Lynch et al. (1995) suggested that this compound is an allosterically acting competitive antagonist of GlyRs. Action of PTX on GABAR channels was also interpreted as the allosteric stabilization of the closed (desensitized) state of the receptor (Newland and Cull-Candy, 1992). However, mutations in the intracellular half of M2 significantly affect the sensitivity of GABARs to PTX (Wang et al., 1995; Zhang et al., 1995a; Curley et al., 1995), the facts compatible with the noncompetitive mechanism of the block. Coexistence of both competitive and noncompetitive mechanisms of the PTX inhibitory action in GABARs has been suggested (Yoon et al., 1993; Qian and Dowling, 1994; Wang et al., 1995).

The blocking activity of CTB and PTX is highly sensitive to the subunit composition of GlyRs and GABARs. Thus, micromolar concentrations of CTB block α_1 and α_1/β but not α_2 GlyRs (Rundström et al., 1994). PTX blocks homomeric α_1 GlyR and ρ_1 $GABA_C$R but weakly antagonizes heteromeric α_1/β GlyR and ρ_1/ρ_2 GABAR (Pribilla et al., 1992; Zhang et al., 1995a). M2s of α_1 and α_2 GlyRs differ only by one residue ($Gly^{2'}$ in α_1 GlyR and $Ala^{2'}$ in α_2 GlyR, see Table 1). Mutation of α_1 $Gly^{2'}$ to Ala makes this receptor insensitive to CTB, suggesting that the ligand binds at the cytoplasmic half of the pore (Rundström et al., 1994).

In the absence of an experimental atomic-scale resolution structure of LGICs, molecular modeling may help suggest mechanisms by which the pore-facing residues affect the functional properties of the channels. Tikhonov and Zhorov (1998) proposed a structural model of nAChR that accommodates various noncompetitive agonists. The model comprises the kinked α-helical M2s that form three regions along the pore: the funnel-like extracellular part, the flexible kinked region comprising conserved $Leu^{9'}$ residues, and a narrow cytoplasmic part where parallel helices may form close contacts with blockers.

In the present study we use this model as a template to built homology models of several GlyRs and GABARs. By using the MCM protocol we have calculated the energy profiles for CTB and PTX in the pore region of the receptors and predicted that these compounds have energetically optimal binding sites in the intracellular half of the pore. We further suggest that the low affinity of CTB and PTX for certain heteromeric receptors is caused by unfavorable contacts between these drugs and the pore-facing residues. These results support the narrow-pore model of LGICs and may help design new mutagenesis experiments and new blockers of Cl^- channels.

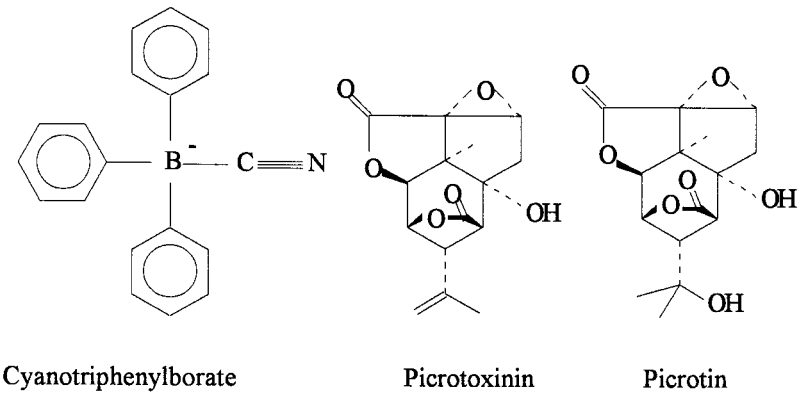

FIGURE 1 Molecular structures of blockers of ligand-gated Cl^- channels.

TABLE 1 Pore-forming segments of ligand-gated and mechanosensitive ion channels

Receptor	Subunit*	Res No†	Positions of the pore-facing residues‡					
			−1′	2′	6′	9′	13′	16′
GlyR	gra1_human	251	**A** R V	**G** L G I	**T** T V	**L** T M T	**T** Q S	**S** G S R
	gra2_human	258	**A** R V	**A** L G I	**T** T V	**L** T M T	**T** Q S	**S** G S R
	grb_human	275	**A** R V	**P** L G I	**F** S V	**L** S L A	**S** E C	**T** T L A
GABA	gar1_rat	307	**A** R V	**P** L G I	**T** T V	**L** T M S	**T** I I	**T** G V N
	gar1_human	306	**A** R V	**P** L G I	**T** T V	**L** T M S	**T** I I	**T** G V N
	gar2_rat	292	**A** R V	**S** L G I	**M** T V	**L** T M S	**T** I I	**T** G V N
	gar2_human	292	**A** R V	**S** L G I	**T** T V	**L** T M T	**T** I I	**T** G V N
	gab3_drome	267	**A** R V	**A** L G I	**T** T V	**L** T M T	**T** I S	**T** G V R
	gab_drome	298	**A** R V	**A** L G V	**T** T V	**L** T M T	**T** L M	**S** S T N
	gab2_mouse	249	**A** R V	**A** L G I	**T** T V	**L** T M T	**T** I N	**T** H L R
	gac2_rat	264	**A** R T	**S** L G I	**T** T V	**L** T M T	**T** L S	**T** I A R
	gaal_mouse§	254	**A** R T	**V** F G V	**T** T V	**L** T M T	**T** L S	**I** S A R
nAChR	acha_torma¶	241	**E** K M	**T** L S I	**S** V L	**L** S L T	**V** F L	**L** V I V
	ach7_bovin	257	**E** K I	**S** L G I	**T** V L	**L** S L T	**V** F M	**L** L V A
MscL‖	1msl**	21	**V** V I	**G** T A F	**T** A L	**V** T K F	**T** D S	**I** I T P

*Names of the subunits given in the SwissProt databank format designate the following proteins: gra1, α_1 GlyR; gra2, α_2 GlyR; grb, β GlyR; gar, ρ_1 GABAR, gar2, ρ_2 GABAR; gaa1, α_1 GABAR; gab2, β_2 GABAR; gac2, γ_2 GABAR; acha_torma, AChR from Torpedo mormorata; GAB3_DROME, Drosophila melanogaster $GABA_AR$, β subunit (gene LCCH3); GAB_DROME, Drosophila melanogaster $GABA_AR$, β subunit (cyclodiene resistance protein, gene RDL).

†The number of the initial residue (position −1′) in the SwissProt databank after deleting the putative signal peptide.

‡According to the numbering scheme of, e.g., Lester (1992). Shown in bold are the pore-facing residues in positions −1′, 2′, 6′, 9′, 13′, and 16′ that correspond, respectively, to the intermediate, threonine, serine, equatorial, valine, and outer leucine rings in nAChRs. Since aligned sequences of the cation-selective and anion-selective LGICs may have essentially different residues in equivalent positions, we designate the rings by the numbers of the corresponding residues rather than by the names.

§The pore-lining residues as determined by Xu and Akabas (1996) using the substituted-cysteine accessibility method are underlined. Residues are numbered as in the paper of Xu and Akabas (1996).

¶Underlined are the pore-lining residues in the nicotinic acetylcholine receptor (Akabas et al., 1994).

‖Pore-forming TM segment of the mechanosensitive channel from Mycobacterium tuberculosis with the known crystallographic structure (Chang et al., 1998).

**Index in the Protein Data Bank.

METHODS

Designating rings of the pore-facing residues

In nAChRs, the rings of pore-facing conserved residues are named after these residues, e.g., *threonine* ring (see Galzi and Changeux, 1995). However, in other LGICs, aligned positions do not necessarily have the same residues. For example, GlyRs have Gly and Pro residues in the positions aligned with the *threonine* ring of nAChRs (see Table 1). This causes a problem in naming the rings in the superfamily of LGICs. In an attempt to solve this problem, we designate the rings by the symbol "R" with a superscript referring to the position of the corresponding residue according to the numbering scheme used by Lester (1992). Thus, $R^{-1'}$, $R^{2'}$, $R^{6'}$, $R^{9'}$, $R^{13'}$, and $R^{16'}$ denote, respectively, the rings aligned with the *intermediate, threonine, serine, equatorial, valine*, and *outer leucine* rings in nAChRs (Table 1 and Fig. 2).

Structure of blockers

CTB is a permanently charged anion, the negative charge evidently promoting binding in the anion-selective pore. The blocker has a star-like shape with three phenyl rings extending from the central boron atom and a CN group capable of accepting H-bonds (Fig. 1). Repulsion between Ph rings hinders rotation around the B-Ph bonds, making CTB a relatively rigid molecule in which only limited conformational changes are possible.

A plant alkaloid, picrotoxin, consists of two compounds, PTX and PTN, which differ only by one group extending from a six-membered ring (Fig. 1). PTX is more potent than PTN in antagonizing effects of GABA (Jarboe et al., 1968; Curtis and Johnston, 1974) and in inhibiting GABA-gated Cl^- channels (Anthony et al., 1994; Shirai et al., 1995). Unlike the negatively charged CTB, PTX is a neutral molecule lacking ionizable groups. PTX has a rigid pentacyclic core with methyl, hydroxyl, and isopropenyl groups capable of rotating around the single bonds attaching them to the core. This compound has an egg-like shape with the isopropenyl group at the elongated end. The rounded end of PTX is trimmed by three ether oxygens and two carbonyl oxygens that may accept but not donate H-bonds. A hydroxyl group decorates the hydrophobic side surface of PTX.

General features of the models

In the present homology modeling study we have used as a template the predicted five-helix-bundle structure of nAChR (Tikhonov and Zhorov, 1998). We did not try to improve the spatial disposition of M2s, their backbone geometry and conformations of the flexible residues extending outside the pore. The borders of the M2s were specified as in the template. The sequences of the M2s are shown in Table 1. Heteromeric models were arranged in the $(\alpha_1)_3/(\beta)_2$ stoichiometry (Langosch et al., 1988). The overall topography of the template was preserved by restraining C^α atoms with the help of pins. A pin is a flat-bottom parabolic penalty function that increases with deviation of a C^α atom by >1 Å from the position specified in the template. A force constant of 10 kcal · mol^{-1} · $Å^{-1}$ was used for the pins.

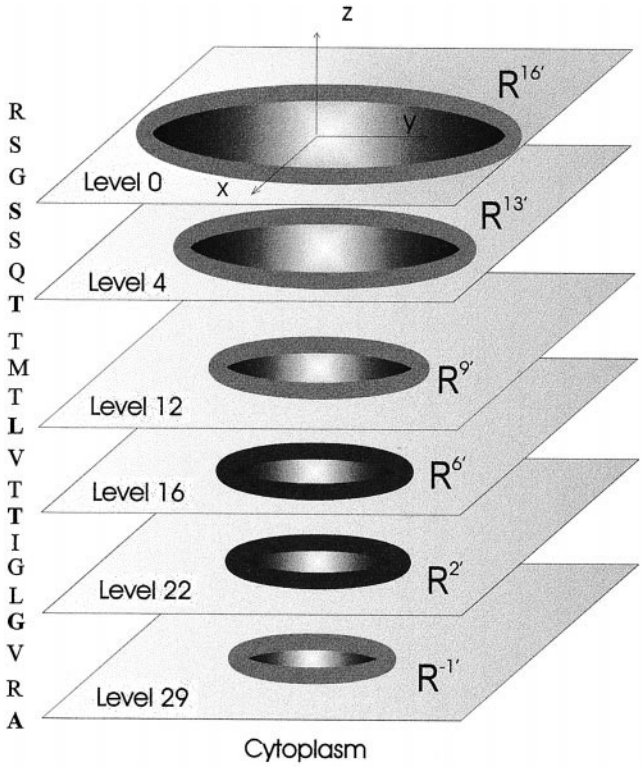

FIGURE 2 A schematic view of the rings of the pore-facing residues in ligand-gated ion channels. Planes represent the pore levels near the rings. Relative dimensions of the rings and distances between the planes at the scheme do not exactly match the computational models. Amino acid sequence of the pore-forming segment M2 of α_1 GlyR is shown as a column that should be read from the bottom to the top.

Software and force fields

All calculations have been carried out using the ZMM program described elsewhere (Zhorov, 1981; Zhorov and Ananthanarayanan, 1996). The program allows conformational searches in the space of arbitrarily specified internal coordinates such as torsion and bond angles, positions of free molecules (Cartesian coordinates of their root atoms), and the orientation of the molecules (Euler angles of the local systems of coordinates centered at the root atoms). Atom-atom interactions were calculated using the AMBER force field (Weiner et al., 1984) with a cutoff distance of 8 Å and a shifting function (Brooks et al., 1985). The energy components most sensitive to the chemical structure of a blocker, its conformation and position in the pore, are van der Waals interactions, hydrogen bonds, and electrostatic interactions involving polar groups. Therefore, we have ignored solvating effects and used Coulomb law for the calculations of the electrostatic energy. Since the charges at the ionizable residues should be compensated by counterions whose location is unknown, we considered all the ionized residues in their neutral forms, as was proposed by Momany et al. (1975). The standard atomic charges of amino acids with a distance-dependent dielectric parameter were used (Weiner et al., 1984). The partial charges at the atoms of blockers were calculated with the MOPAC software (Biosym Inc., San Diego, CA, USA). In most of the computational experiments, the CH, CH_2, and CH_3 groups of the receptor and CH groups of CTB were represented by united atoms specified in the AMBER force field. Since boron is not specified in the AMBER force field, its van der Waals interactions were calculated using parameters for a C_{sp3} atom, while the length of the B-C bond was assigned 1.57 Å based on the respective covalent radii of 0.80 and 077 Å. Quantum-chemical calculations of CTB yielded charges of −0.13, 0.05, and −0.29 proton charge units, respectively, for B, C, and N atoms in the B-CN group, a charge of −0.63 units being distributed over three phenyl rings to yield a net CTB charge of −1 unit.

MCM protocol

For the search of optimal conformations the MCM protocol (Li and Scheraga, 1988) was used as described elsewhere (Zhorov and Ananthanarayanan, 1996). Trajectories were calculated at $T = 600$ K. A subsequent starting point in a trajectory was obtained by changing a randomly selected internal coordinate of the preceding point by a random increment. In the MCM calculations of ligand-free receptors, all internal coordinates were sampled. In the MCM calculations of the energy profiles, a list of internal coordinates to be sampled was formed and then updated periodically. It included generalized coordinates of the blocker and torsions of the receptor residues around the blocker (see below). From a given starting point, the energy was minimized until the norm of the energy gradient become <1 kcal · mol^{-1} · rad^{-1} or a limit of 200 calls to the procedure of the gradient calculation was exceeded. The resulting MEC was accepted in the trajectory if its energy E was less than that of the preceding point of the trajectory E_p or if a random number $n \in (0, 1)$ was $<\exp((E-E_p)/RT)$. The obtained MEC was added to an internal stack (array) of MECs accumulated during the search if its energy did not exceed 7 kcal/mol above the lowest-energy structure in the stack and if it was geometrically distinct from any other MEC accumulated in the stack (Zhorov and Ananthanarayanan, 1993). Two MECs were considered distinct if they had a different backbone code (Zimmerman et al., 1977) or a side-chain torsion angle different by at least 10°. For the molecular systems under consideration, the internal stack had a capacity of 40 MECs. If and when the internal stack overflowed, its content was delivered to the external stack (file). After this procedure, redundant MECs and those with an energy above 7 kcal/mol from the lowest-energy MEC were removed from the internal and external stacks. A trajectory was terminated if 500 consecutive energy minimizations did not decrease the energy of the best MEC found nor added a new MEC to the internal stack. When calculating energy profiles, only the lowest-energy MEC found in each MCM trajectory was preserved for further analysis. These trajectories were usually terminated if 500 consecutive energy minimizations did not decrease the energy of the best MEC, but a large number of different MECs repeatedly overflowed the internal stack.

Positions 0′, 11′, 14′, and 19′ in M2s of GlyRs and GABARs comprise long-chain residues which are either at the borders of M2 or do not face the pore. Test MCM trajectories with all degrees of freedom sampled with equal probability converged slowly and yielded large external stacks of MECs with different orientations of the above residues. To speed up the convergence of standard trajectories, no MC sampling was performed for positions and orientations of M2s, all backbone torsions, and the side-chain torsions in positions 0′, 11′, 14′, and 19′. However, all the generalized coordinates were varied in energy minimizations.

MC-minimized energy profiles

A special procedure was elaborated to pull a ligand through the pore. The pore axis is oriented along the $-z$ axis of the Cartesian coordinate system with ring $R^{16'}$ close to the xy plane; other rings having negative z coordinates (Fig. 2). A position of a ligand along the pore is specified by z_R, the z coordinate of its root atom. The root atom of CTB is the tetrahedral carbon; the root atom of PTX is the central carbon shared by two five-membered rings and the six-member ring (Fig. 1). When z_R is fixed, the ligand is restrained at the given level of the pore. However, it may rotate around the root atom and move normally to the pore axis so that an MCM trajectory would yield an optimal position and orientation of the ligand at the given level of the pore. To build the MC-minimized energy profile of a ligand in the pore, a series of MCM trajectories with the z-constrained ligand were calculated and the lowest-energy structures were collected

from each trajectory. Test MCM trajectories which were started from the same z_R, other internal coordinates being different, converged to similar but not identical structures. To minimize the dependence of an MC-minimized structure on the starting geometry, we have used the same starting geometry of the receptor and the same orientation of the ligand for the given series of MCM trajectories.

Each receptor model was initially optimized by a long MCM trajectory in the absence of a ligand with all side-chain torsions being sampled. To speed up calculations of energy profiles, we used the optimized structures of the receptors as the starting points and sampled only those variables that affect the ligand-receptor interactions by governing conformation, position, and orientation of the ligand and conformations of the residues close to the ligand. According to the standard ZMM protocol, each 50th energy minimization rebuilds an interaction list that includes pairs of atoms at less than the cutoff distance (8 Å in this study). Simultaneously, the list of variables to be sampled was rebuilt to include all degrees of freedom of the ligand and those side-chain torsions that govern positions of atoms within 8 Å from the ligand. The side-chain torsions were sampled using the biased probability MCM protocol (Abagyan and Totrov, 1994).

RESULTS

Background of the models

In the absence of a high-resolution structure of LGICs, we have built homology models of GlyRs and GABARs using as a template the model of nAChR that explained structure-activity relationships of noncompetitive blockers (Tikhonov and Zhorov, 1998). The template consists of five α-helical M2 segments kinked in their middle part. The helices are parallel to each other in positions $-1'$ to $9'$, but diverge at position $9'$ to $19'$ to make a funnel-like pore. The C^α atoms at positions $-1'$, $2'$, $6'$, $9'$, $13'$, and $16'$ face the pore. Residues in these positions were experimentally determined to line the pore in both cation-selective and anion-selective LGICs (Akabas et al., 1994; Xu and Akabas, 1996; footnotes § and ¶ in Table 1). This fact justifies using the model of nAChR as a template for homology models of chloride-selective LGICs. In the homology models, the C^α atoms are restrained to the template by pins, while side chains may move to adjust ligands.

Below we present the MC-minimized energy profiles for CTB and PTX in the homomeric and heteromeric Cl^--selective GlyRs and GABAR. We further analyze interactions that stabilize the optimal ligand-receptor complexes and discuss structure-function relationships of the ligand and ion channels in view of the obtained results.

Locating optimal binding sites for blockers in the pore

In our models, the pore axis coincides with the $-z$ axis of the Cartesian system of coordinates, the plane xy being close to ring $R^{16'}$ (see Fig. 2 and Table 3). To locate optimal binding sites for CTB and PTX, we have pulled the ligands through the pore from ring $R^{16'}$ to ring $R^{-1'}$ with the step of 1 Å (from level 0 to level 29; see Fig. 2). At each level, an MCM trajectory was calculated with the z coordinate of the ligand's root atom being fixed and all other variables allowed to vary. The backbone topology of the pore was preserved by pinning C^α atoms. The following parameters of the lowest-energy MEC found in each trajectory were used to draw the energy profiles: the total energy E_t, the energy of ligand-receptor interactions E_{lr}, and electrostatic component of the energy of ligand-receptor interactions, E_{lre}.

With given starting geometry and parameters controlling an MC protocol, the energy E_t depends on the length of the trajectory. The top, middle, and bottom lines at Fig. 3 *A* show E_t obtained, respectively, after a single energy minimization, after 100 energy minimizations, and after the trajectory converged. (A usual reason for the convergence was repeated overflowing of the internal stack of MECs without decreasing E_t during 500 consecutive energy minimizations, see Methods.) An MCM trajectory takes 700-3300 minimizations (Fig. 3 *B*) while obtaining one MCM

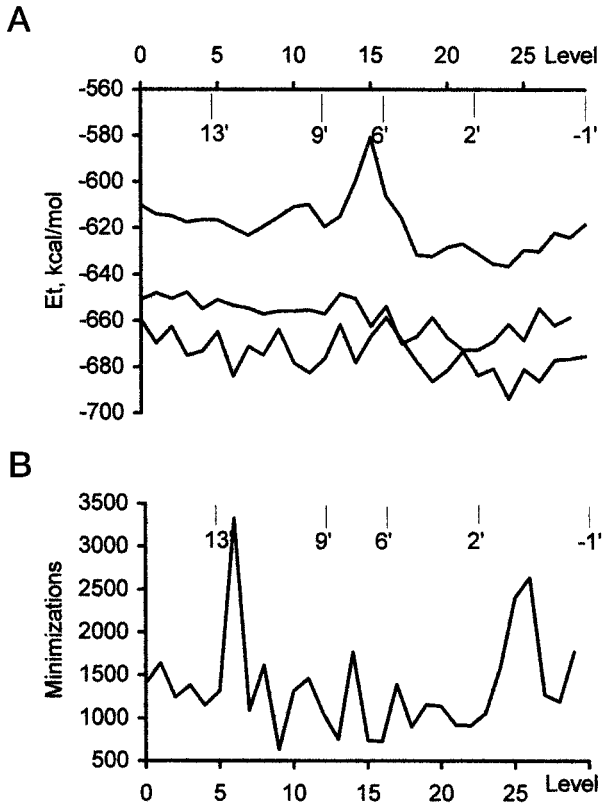

FIGURE 3 (*A*) Energy profiles of E_t for CTB in α_1/β GlyR. The top, middle, and bottom thin lines show energies obtained after single minimization at each level, after 100 minimizations, and upon the convergence of the MCM trajectory (when the internal stack of MECs repeatedly overflowed without decreasing the lowest energy during 500 minimizations). Positions of rings of the pore-facing residues $R^{-1'}$, $R^{2'}$, etc. along the pore are indicated by labeling levels accommodating C^α atoms of the corresponding residues (see Table 3). (*B*) The number of energy minimizations performed upon the convergence of the trajectories.

energy profile requires more than 30,000 minimizations. With the reference to the energy-minimized starting points (the top line in Fig. 3 *A*), the initial 100 minimizations decrease E_t by 30–40 kcal/mol while the converged trajectories decrease E_t by 60–80 kcal/mol. Since an MCM trajectory is not expected to reach the global minimum, the ragged shape of the profiles of E_t most probably reflect incomplete optimizations rather than essentially different ligand-receptor interactions at adjacent levels of the pore. Indeed, the profiles of E_{lr} are smoother than those of E_t (see Fig. 4, *A–E*) indicating that bad ligand-receptor contacts occurring after inserting the ligand at the given level of the pore relax faster than bad intra-receptor contacts. The latter occur as the pore-facing residues move away from the

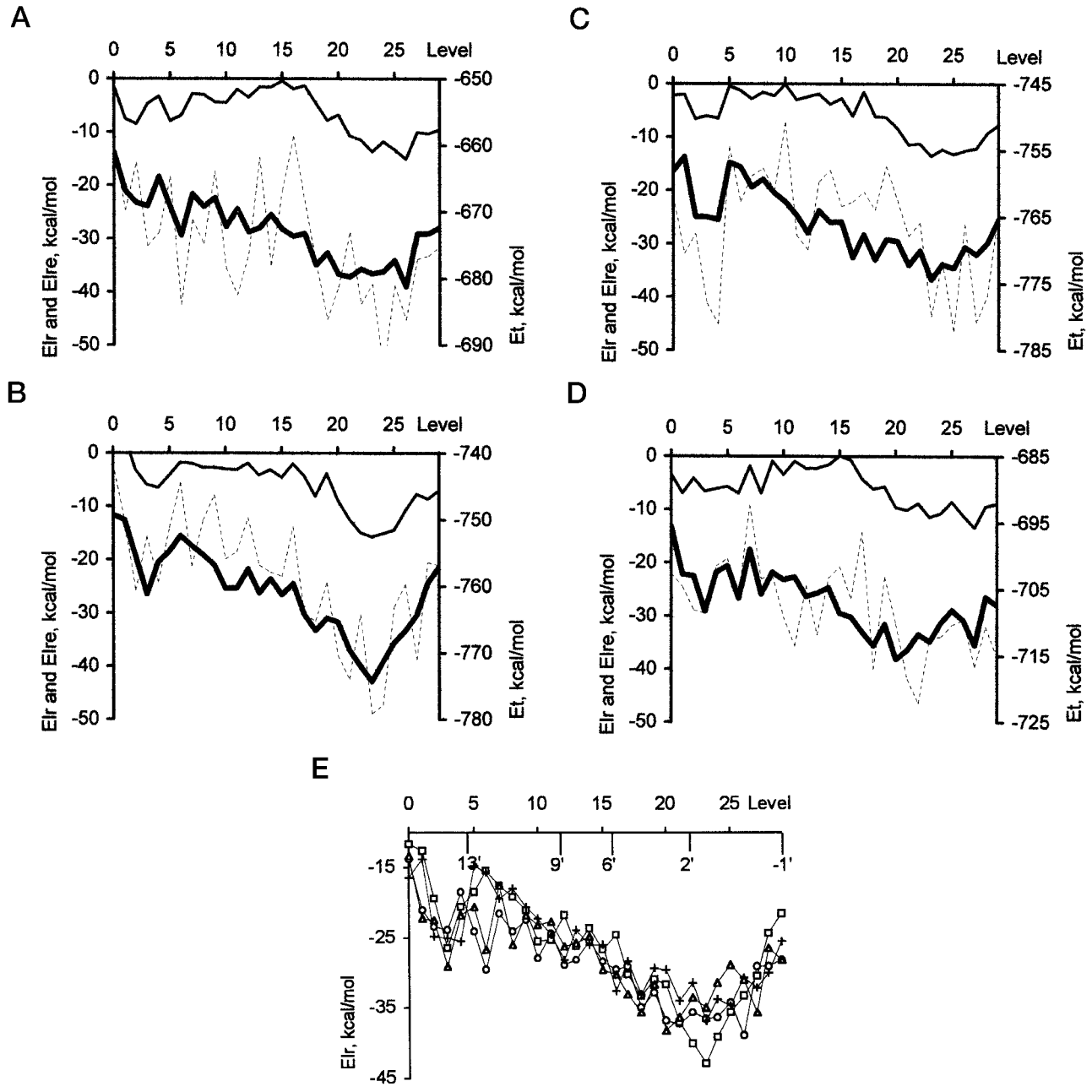

FIGURE 4 MC-minimized energy profiles of CTB in the α_1/β (*A*), α_1 (*B*), α_2 (*C*), and α_2/β (*D*) GlyRs. The profiles represent the total energy E_t (*dashed line*), ligand-receptor energy E_{lr} (*bold line*), and E_{lre}, the electrostatic component of E_{lr} (*thin line*). (*E*) Superposition of the E_{lr} profiles shows the deepest minimum for α_1 GlyR (*squares*) and the second deep minimum for α_1/β GlyR (*circles*). The minimum for α_2/β GlyR (*triangles*) is shifted toward ring $R^{6'}$, indicating that CTB does not interact properly with ring $R^{2'}$. The energy minimum at the profile of CTB in for α_2 GlyR (*crosses*) is both shallow and narrow as compared with other receptors. This is consistent with the low activity of CTB at α_2 GlyR (see Table 2). Positions of rings of the pore-facing residues $R^{-1'}$, $R^{2'}$,etc. along the pore are indicated by labeling levels accommodating C^{α} atoms of the corresponding residues (see Table 3).

ligand at initial minimizations. These residues may be trapped at high-energy levels because the pinned C^{α} atoms lack the mobility necessary to bypass energy barriers and reach low-energy valleys. In contrast, bad ligand-receptor contacts relax faster because only the z coordinate of the root atom of the ligand is constrained.

CTB in GlyRs

As summarized in Table 2, CTB effectively blocks α_1 and α_1/β GlyR with IC_{50} 1.3–2.8 μM. In contrast, CTB is inactive in α_2 GlyR whose M2 differs from that in α_1 GlyR by only one residue: $Gly^{2'}$ in α_1 GlyR and $Ala^{2'}$ in α_2 GlyR (Table 1). The mutation of $Gly^{2'}$ in the α_1 GlyR to Ala yields receptors resistant to the CTB block (Rundström et al., 1994), clearly indicating that methyl groups of the five $Ala^{2'}$ residues impede CTB binding. To understand structural reasons for these experimental data, we have calculated MC-minimized energy profiles of CTB in heteromeric (α_1/β and α_2/β) and homomeric (α_1 and α_2) GlyRs.

CTB in α_1/β GlyR

The MC-minimized energy profile for CTB in α_1/β GlyR (Fig. 4 *A*) has deep and wide minima of E_{lr} and E_{lre} between levels 20 and 26. At level 24, a minimum of E_{lr} coincides with a deep minimum of E_t indicating that ligand-receptor interactions do not conflict with the intrareceptor interactions or the pins. At levels 21–24, the ligand fits between α_1 $Gly^{2'}$ and β $Pro^{2'}$ residues (Fig. 5). The profile of E_t has a barrier at level 16, close to ring $R^{6'}$. Fig. 6 shows three snapshots of CTB passing ring $R^{6'}$. At level 14, a phenyl group of CTB intrudes between $Phe^{6'}$ and $Thr^{6'}$ residues in adjacent M2s. A dramatic change of CTB orientation is seen at level 15 as two phenyl groups of CTB squeeze between side chains of $Phe^{6'}$ and $Thr^{6'}$ residues, while the third phenyl group of CTB remains at the extracellular side of ring $R^{6'}$. As CTB proceeds to level 16, side chains of $Phe^{6'}$ residues move back toward the pore axis while a repulsion of CTB from three $Thr^{6'}$ residues increases E_t (see Fig. 4 *A*). Thus, the MC-minimized energy profile predicts that a relatively large CTB may pass ring $R^{6'}$ and reach ring $R^{2'}$. This explains why mutations of M2s at position 2′ affect CTB binding (see Table 2).

CTB in α_1 GlyR

The MC-minimized energy profiles of CTB in α_1 GlyR (Fig. 4 *B*) show minima of E_t, E_{lr}, and E_{lre} at level 23, close

TABLE 2 Activity of chloride channel blockers at glycine and GABA receptors

Ligand	Receptor	Subunit	IC_{50} (μM)	Reference	Rings†	
					$R^{2'}$	$R^{6'}$
CTB	GlyR human	α_1	1.3–2.6	Rundström et al., 1994	G	T
		$\alpha_1 + \beta$	2.8	"	G, P	T, F
		$\alpha_2 + \beta$	7.5	"	A, P	T, F
		$\alpha_2 + \beta$*	3.0	"	A, A*	T, F
		α_1*	>>20	"	A*	T
		α_2	>>20	"	A	T
PTX	GlyR human	α_1	9	Pribilla et al., 1992	G	T
		α_2	6	"	A	T
		$\alpha_1 + \beta$	>1000	"	G, P	T, F
		$\alpha_2 + \beta$	300	"	A, P	T, F
		$\alpha_1 + \beta$*	~10	"	G, G*	T, T*
		α_1	62	Lynch et al., 1995	G	T
PTN	GlyR human	α_1	57	Lynch et al., 1995	G	T
PTX	$GABA_c$ human	ρ_1	1–50	Wang et al., 1994, 1995	P	T
		ρ_1*	4.8	"	S*	T
		ρ_1*	5.8	"	G*	T
		ρ_1*	0.1	"	A*	T
		ρ_2	4.7	"	S	T
		$\rho_1 + \rho_1$*	4.8	"	S, P*	T
		ρ_1	5.5	Enz and Bormann, 1995	P	T
		ρ_1*	21	"	S*	T
PTX	$GABA_C$ rat	ρ_1	1.0	Zhang et al., 1995b	P	T
		$\rho_1 + \rho_2$	100	"	P, S	T, M
		$\rho_1 + \rho_1$*	1000	"	P	T, M*
	$GABA_A$ rat	$\alpha_1 + \beta_2 + \gamma_2$	1.3	Curley et al., 1995	V, A, S	T
		α_1* $+ \beta_2 + \gamma_2$	>100	"	V, A, S	T, F*
		$\alpha_1 + \beta_2$* $+ \gamma_2$	>100	"	V, A, S	T, F*
		$\alpha_1 + \beta_2 + \gamma_2$*	>100	"	V, A, S	T, F*

*Mutated residues.
†The rings of the pore-facing residues $R^{2'}$, $R^{6'}$ aligned, respectively, with threonine and serine rings in nAChR.

TABLE 3 Rings of the pore-facing residues

Ring	Residue*	Coordinates of C^{α} atom†, Å			Nearest plane‡ to which the root atom of the ligand is constrained	
		x	y	z	Level	z, Å
$R^{16'}$	Gly^{269}	−12.746	6.607	−0.653	0	0
$R^{13'}$	Thr^{265}	−11.278	2.072	−4.296	4	−4
$R^{9'}$	Leu^{261}	−9.285	−1.591	−11.776	12	−12
$R^{6'}$	Thr^{258}	−6.569	−0.587	−15.882	16	−16
$R^{2'}$	Gly^{254}	−6.428	−0.791	−21.948	22	−22
$R^{-1'}$	Ala^{251}	−9.539	0.095	−29.301	29	−29

*In one M2 segment. Other M2s are arranged quasi-symmetrically around the z axis. No symmetry operations were used during sampling variables, calculating energies, and performing movements.

†As calculated in the MC minimized model of non-liganded α_1 GlyR.

‡The planes nearest to the C^{α} atoms in the rings of the pore-facing residues. A total of 30 planes spaced by 1 Å were used to constrain ligands' root atoms during calculations of the energy profiles.

to $Gly^{2'}$ residues. Five β-branched side chains of $Thr^{6'}$ residues in α_1 GlyR would be expected to form a higher barrier for CTB as compared to α_1/β GlyR, in which $Phe^{6'}$ residues move away to give room for CTB (see Fig. 6). However, the wide ring of $Gly^{2'}$ residues in the α_1 GlyR provides room for CTB to maneuver as it passes the $Thr^{6'}$ ring (note a small barrier of E_t at level 16, Fig. 4 *B*). Thus, in accordance with the experimental data (Table 2) the MC-minimized energy profile predicts binding of CTB at the ring of $Gly^{2'}$ residues in α_1 GlyR.

CTB in α_2 GlyR

The MC-minimized energy profiles of CTB in α_2 GlyR (Fig. 4 *C*) show minima of E_t at levels 4 and 23 and barriers

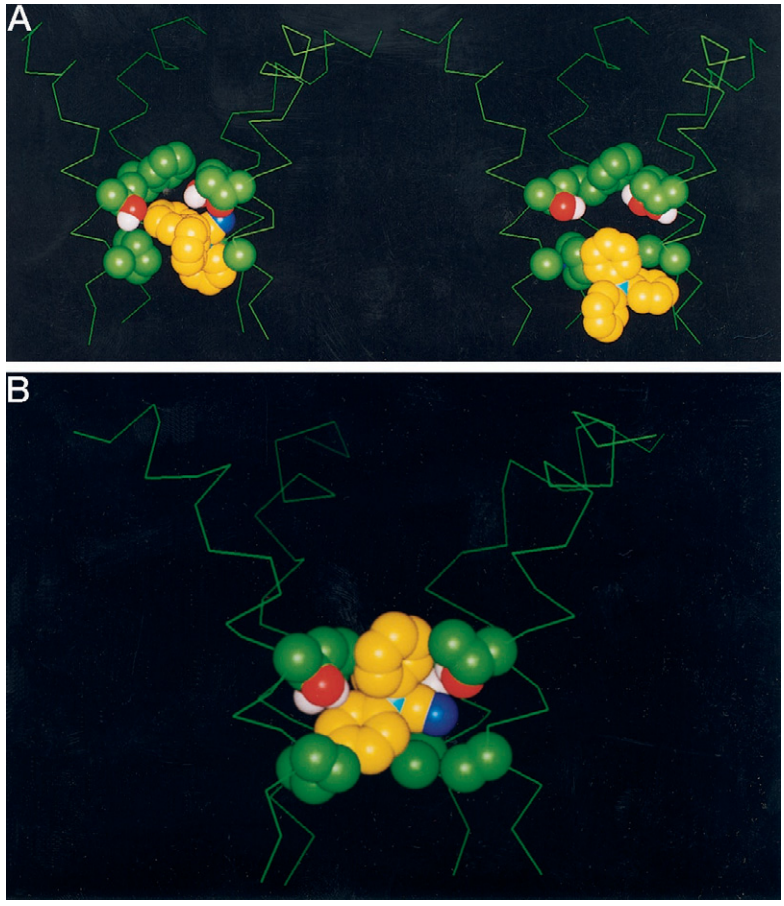

FIGURE 5 Complexes of CTB with GlyRs. The ligand and side chains in the rings of pore-facing residues near the ligand are space-filled. Carbon, nitrogen, and boron atoms of CTB are colored yellow, blue, and light blue, respectively. One M2 segment is removed for a better view of the ligand. (*A*) CTB at levels 21 (*left*) and 24 (*right*) of the α_1/β GlyR corresponding to two points in the deep and wide minimum of the profile E_{lr} at Fig. 4 *A*. (*B*) CTB at level 19 of the α_2 GlyR corresponding to the barrier of E_t at Fig. 4 *C*. CTB is squeezed between rings $R^{6'}$ and $R^{2'}$, and lacks the room to maneuver and pass the barrier as readily as in the α_1/β GlyR (see Fig. 6).

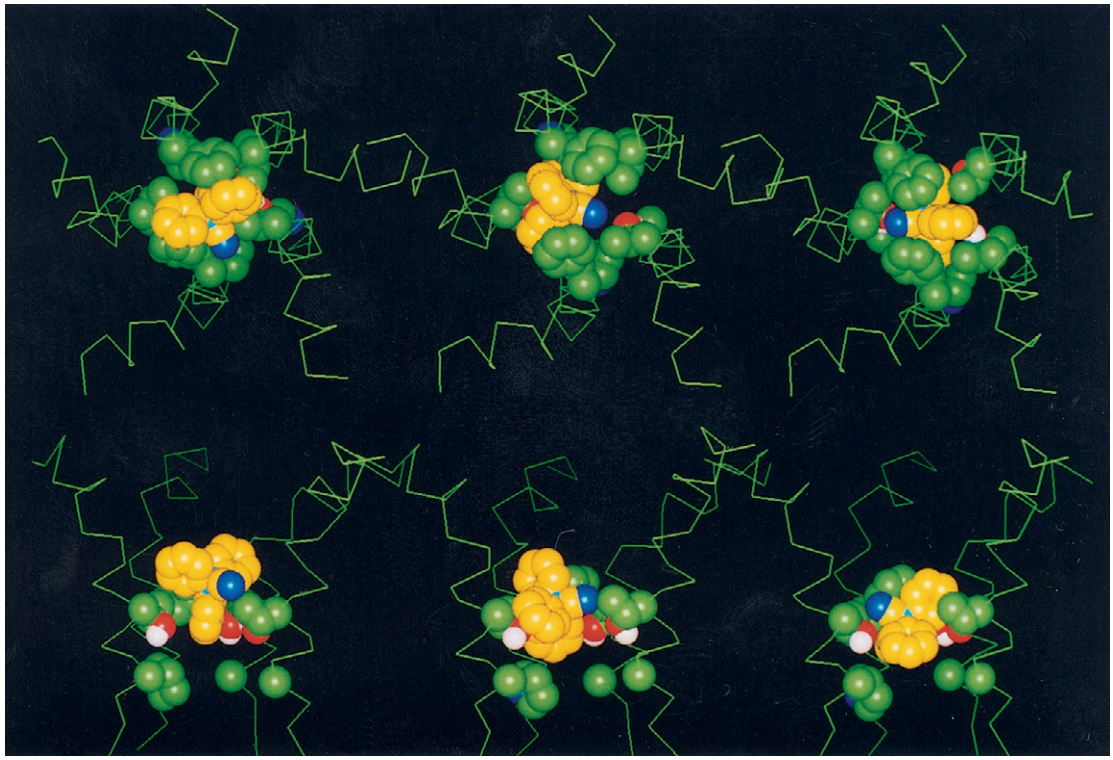

FIGURE 6 Extracellular and side views of CTB passing ring $R^{6'}$ in α_1/β GlyR. Three rows, left to right, correspond, respectively, to levels 14–16. At side views, one M2 segment is removed for a better view of the ligand. See text for further explanation.

at levels 10 and 13–22. The minimum at level 4 (present also at CTB profiles in other GlyRs) is due to the intercalation of the ligand between two diverging M2s. In real GlyRs, M1s that contribute to the synaptic end of the pore (Akabas and Karlin, 1995) would obstruct such intercalation. The minimum of E_t at level 23 is shallower and narrower than the corresponding minima for α_1 and α_1/β GlyRs (Fig. 4 *E*). This factor may contribute to the low activity of CTB in α_2 GlyR.

In general, the barriers of E_t in α_2 GlyR are essentially higher than in α_1 and α_1/β GlyRs. The barrier at level 10 is due to incomplete optimization: α_1 GlyR has the same residues but does not have a barrier of E_t at this level. However, the wide barrier at levels 13–22 has a physical reason: at level 19, CTB is squeezed between the rings of $Thr^{6'}$ and $Ala^{2'}$ residues (Fig. 5 *B*). The blocker lacks space to maneuver and cannot adjust its phenyl rings between $Thr^{6'}$ residues as in α_1 GlyR. Since the permanently charged CTB cannot pass via the lipid bilayer to reach the binding site from inside the cell, the barrier in the pore may contribute to the low activity of CTB at the α_2 GlyR.

CTB in α_2/β GlyR

Heteromeric α_2/β GlyR with $Ala^{2'}/Pro^{2'}$ and $Thr^{6'}/Phe^{6'}$ residues is blocked by CTB rather effectively, with IC_{50} of 7.5 μM (Table 2). This fact is surprising because CTB does not block α_2 GlyR, whose ring of $Ala^{2'}$ residues is not expected to be wider than the ring of $Ala^{2'}/Pro^{2'}$ residues in α_2/β GlyR. Moreover, substitution of $Pro^{2'}$ by $Ala^{2'}$ in the β GlyR subunit failed to abolish the inhibitory activity of CTB (Rundström et al., 1994) indicating that $Pro^{2'}$ residues in α_2/β GlyR do not increase the affinity for the blocker. These observations also suggest that residues other than 2′ may contribute to the inhibitory action of CTB. Indeed, Table 2 shows that rings $R^{2'}$ and $R^{6'}$ concertedly affect CTB activity: five $Ala^{2'}$ and five $Thr^{6'}$ residues impede the CTB binding, whereas the presence of $Phe^{6'}$ residues promote CTB binding despite the five $Ala^{2'}$ residues.

To understand these paradoxical facts, we have calculated the MC-minimized energy profiles of CTB in α_2/β GlyR (Fig. 4 *D*) and found the minimum of E_{lr} to be deeper and the barrier of E_t to be narrower than in α_2 GlyR (see superimposed profiles in Fig. 4 *E*). The results suggest that unlike the rings of $Thr^{6'}$ and $Ala^{2'}$ residues in α_2 GlyR, the rings of $Phe^{6'}/Thr^{6'}$ and $Ala^{2'}/Pro^{2'}$ residues in the α_2/β GlyR provide enough room for CTB to maneuver, helping the blocker to reach the low-energy binding site at ring $R^{2'}$. Thus, our calculations provide a possible explanation for the paradoxical relationships between the activity of CTB and the structure of M2s at positions 2′ and 6′.

PTX in GlyRs

PTX effectively inhibits ionic currents in the homomeric human α_1 and α_2 GlyRs with IC_{50} of 6–9 μM, but displays a low affinity for the heteromeric α_1/β GlyR (Table 2). Test calculations of PTX in GlyR with MCM trajectories, run under standard controlling parameters, yielded a ragged profile of E_t (not shown) because the bulky ligand induced many unfavorable intrareceptor contacts in the initial steps. Relaxation of these contacts required long MCM trajectories that smoothed the E_t profile but did not significantly change the E_{lr} profile because, as mentioned above, bad ligand-receptor contacts relax faster than bad intrareceptor contacts. Therefore, the MCM energy profiles for PTX are represented only by the ligand-receptor energy E_{lr} and by its electrostatic component E_{lrt}. Those degrees of flexibility that are not considered in our model (e.g., flexible bond angles) would smooth the profiles of E_t.

PTX in α_1 GlyR

The E_{lr} profile has minima at levels 12–14 and 19–24 and a barrier of ~8 kcal/mol at levels 15–18 (Fig. 7 *A*). At level 13, the long axis of PTX is normally oriented to the pore axis. The methyl group protruding from PTX side fits the hydrophobic ring formed by the methyl groups of $Thr^{6'}$ residues, while carbonyl and ether oxygens of PTX accept H-bonds from three $Thr^{10'}$ residues and an isopropenyl group approaches two other $Thr^{10'}$ residues (not shown). A barrier of E_{lr} is observed at levels 15–18. At level 17, the long axis of PTX is parallel to the pore axis (Fig. 8 *A*), the H-bond between $Thr^{6'}$ and PTX hydroxyl decreasing the barrier. The energetically preferable binding mode is observed at level 21, where the rounded end of PTX accepts H-bonds from $Thr^{6'}$ residues (Fig. 8 *B*). Since our calculations do not take into account solvent effects, they underestimate the stabilizing energy of H-bonds between PTX and $Thr^{6'}$ residues at the narrow level 21, where the ligand would displace most of the intrapore waters. Unlike the anionic CTB, the electroneutral PTX does not interact with the helical macrodipole, yielding the E_{lre} profile without a deep minimum at the cytoplasmic end. However, attraction of the negatively charged PTX oxygens to the positively charged C′ atoms of the peptide backbone determine the negative values of E_{lre} all along the pore.

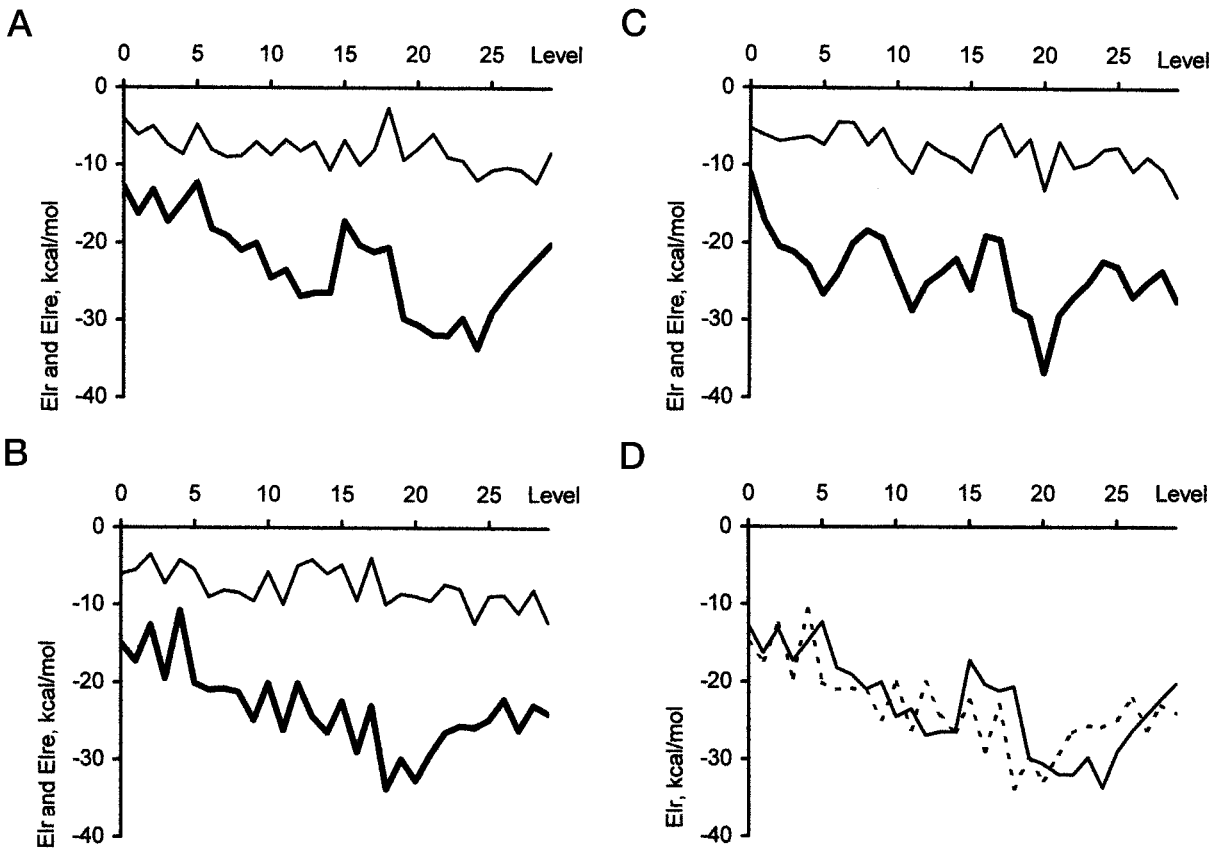

FIGURE 7 MC-minimized energy profiles of PTX in the α_1 GlyR (*A*), α_1/β GlyR (*B*), and in ρ_1 GABAR (*C*) showing the ligand-receptor energy E_{lr} (*bold line*), and E_{lre}, the electrostatic component of E_{lr} (*thin line*). (*D*) Superposed E_{lr} profiles from the plots (*A*) and (*B*) show that the minimum of the PTX profile in α_1 GlyR is wider and deeper than in α_1/β GlyR (*dotted line*).

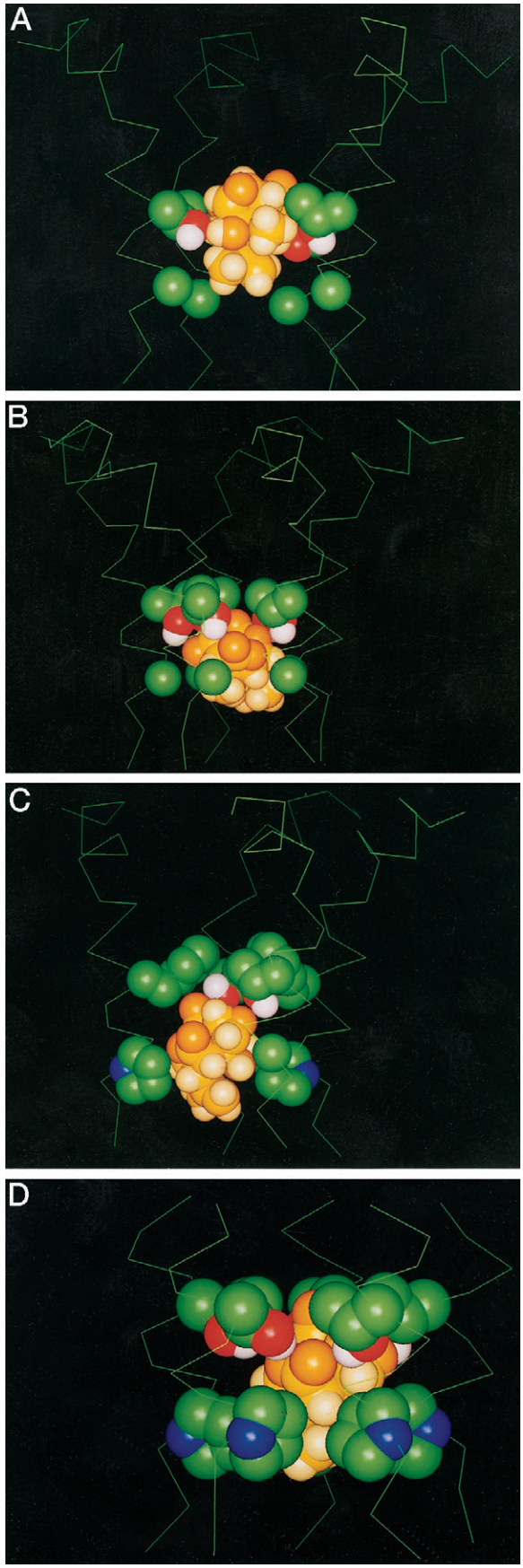

PTX in α_1/β GlyR

The MC-minimized energy profile of E_{lr} for α_2/β GlyR has a minimum at levels 18–20 (Fig. 7 *B*). Superposition of the E_{lr} profiles for PTX (Fig. 7 *D*) shows that the minimum in α_1/β GlyR is narrower than in α_1 GlyR and is shifted by ~5 Å toward the $R^{6'}$ ring. At level 21, PTX fits between rings $R^{6'}$ and $R^{2'}$. Only three $Thr^{6'}$ residues may donate H-bonds to the PTX oxygens because $Phe^{6'}$ residues lack H-bond donors in the side chain (Fig. 8 *C*). This may be the major factor impeding PTX activity in the α_1/β GlyR.

Thus, our calculations predict that PTX may reach rings $R^{6'}$ and $R^{2'}$ from the extracellular side and accept several H-bonds from the ring of five $Thr^{6'}$ residues present in the homomeric GlyR. Our model explains the low activity of PTX at the heteromeric receptors with β GlyR subunits by the lack of H-bond donors in the side chain of $Phe^{6'}$ residue leading to a weaker interaction of PTX with the channel.

PTX in ρ_1 GABAR

In addition to its blocking action on GlyRs, PTX also antagonizes homomeric and heteromeric GABARs with high to moderate affinities (Table 2). Mutations in positions 6′ and 2′ dramatically affect PTX activity (see Table 2), suggesting that in GABARs the binding site for the blocker is located at the same levels of the pore as in GlyRs. To analyze the impact of the pore-facing residues on the binding of the blocker, we have calculated the energy profile of PTX in the ρ_1 GABAR. Because the united-atom model may underestimate a probable repulsion between five $Pro^{2'}$s and PTX, we have built a more realistic all-atom model of ρ_1 GABAR.

The calculated MCM profile has a deep, narrow minimum at level 20 (Fig. 7 *C*). The MCM trajectory at this level yielded the lowest-energy MEC with the PTX elongated end at ring $R^{2'}$ and the oxygens at the rounded end of PTX accepting H-bonds from $Thr^{6'}$ residues (Fig. 8 *D*). Although the elongated end of PTX fits the ring of five $Pro^{2'}$ residues, C^{β} atoms of $Pro^{2'}$ impede the mobility of the blocker at this level. The observations that substitution of $Pro^{2'}$ in ρ_1 $GABA_CR$ by Ala increases activity of PTX (Table 2) is probably due to the larger $R^{2'}$ ring providing more room for

FIGURE 8 Complexes of PTX with GlyRs and ρ_1 GABAR corresponding to the extreme points of the energy profiles in Fig. 7. PTX and side chains in the rings of the pore-facing residues near PTX are space-filled. Oxygen, carbon, and hydrogen atoms of PTX are colored, respectively, by the dark, normal, and light shades of yellow. (*A* and *B*) PTX at levels 17 and 21 in the α_1 GlyR that correspond, respectively, to the maximum and minimum of the energy profile in Fig. 7 *A*. (*C*) PTX at level 21 of α_1/β GlyR corresponding to the energy minimum of the profile in Fig. 7 *B*. (*D*) PTX at level 20 of ρ_1 GABAR corresponding to the energy minimum of the profile in Fig. 7 *C*. The extracellular parts of M2s, which do not affect PTX binding between rings $R^{2'}$ and $R^{6'}$ are truncated after $Thr^{10'}$.

PTX mobility. Substitution of $Thr^{6'}$ by Phe or Met essentially decreases the PTX activity (Table 2). This concurs with our above conclusion that $Thr^{6'}$ residues in GlyRs stabilize PTX by donating several H-bonds.

Thus, our models qualitatively explain the relationships between the structure of rings $R^{6'}$ and $R^{2'}$ in GABARs and GlyRs, and their sensitivity to PTX. We conclude that the ring of $Thr^{6'}$ residues that may donate several H-bonds to the rounded end of PTX is the key structural determinant of PTX activity at both GlyRs and GABARs.

Hydrated Cl^- in α_1 GlyR

Our calculations suggest that relatively large organic blockers may reach ring $R^{2'}$ from the extracellular side. The pore between rings $R^{16'}$ and $R^{2'}$ should be wide enough to accommodate Cl^- with its inner hydration shell. Since the positively charged hydrogens of water molecules surround Cl^-, the oxygen atoms of the waters would accept H-bonds from the rings of polar residues in a manner that may resemble, to some extent, the interaction of the oxygens at the rounded end of PTX with the H-bond-donating rings. To highlight a possible analogy in the binding of PTX and hydrated Cl^-, we have calculated an MC-minimized energy profile of the cluster $Cl^-/(H_2O)_8$ in the α_1 GlyR. The water oxygens were constrained to Cl^- by the flat-bottom penalty functions with the upper distance limit of 6 Å. As in the case of computing energy profiles for CTB and PTX, the z coordinate of Cl^- was fixed at 30 levels of the pore and MCM trajectories were calculated to find optimal structures of the Cl^- hydration shell, optimal position of Cl^- at the given level of the pore, and optimal side-chain conformations of the receptor. This approach allows Cl^- to exchange waters from its surroundings for more attractive groups in the channel, to abandon waters in the pore constrictions, but rejoin the waters at the wide levels of the pore.

Fig. 9 *A* shows the MC-minimized energy profile of $Cl^-/(H_2O)_8$ in the α_1 GlyR. The lowest-energy structures found in each trajectory are characterized by the total energy (E_t), the energy of interactions of Cl^- with the receptor and waters (E_{Cl}), and E_{Cl_e}, the electrostatic component of E_{Cl} that provides the major contribution to E_{Cl}. E_t is high at levels 0–4 because Cl^--bound waters do not establish favorable contacts with the channel. Eight Cl^--OH_2 distances plotted against the Cl^- position in the pore (Fig. 9 *B*) show that five or six waters approach Cl^- at levels 0–6, while two to six waters remain in a close contact to Cl^- at other levels.

The profiles of E_t and E_{Cl} have maxima at level 17, where most of the water molecules move away from Cl^- (Fig. 9 *B*) to interact with $Thr^{7'}$ residues. The latter are specific for Cl^--selective channels (Table 1) and may contribute to the anionic selectivity. The profile of E_{Cl} below ring $R^{6'}$ (levels 20–24) has deep and wide minimum corresponding to the most preferable binding site for the hydrated Cl^-. The cluster $Cl^-/(H_2O)_8$ at level 22 is extended along the pore as four waters are retarded at $Thr^{6'}$ residues to form a pattern resembling the rounded end of PTX (Fig. 10). The model of Cl^- hydration applied is too simple to account for the anion selectivity of GlyRs and GABARs. However, it shows that $Thr^{6'}$ residues may stabilize the hydrated Cl^- inside the pore in the same manner as they stabilize PTX. This provides a possible explanation for the nature of Cl^- channel block by PTX.

Mechanosensitive receptor and LGICs

Recently, a crystallographic structure of a mechanosensitive ion channel (MscL) was published (Chang et al., 1998). It shows a five-helix bundle forming the central pore with the crossing angle between the pore helices similar to that observed in the KcsA K^+ channel (Doyle et al., 1998). Ligand-gated and mechanosensitive ion channels have a different numbers of TM segments (20 and 10, respectively) and very different electrophysiological properties (Imoto et al., 1988; Newland and Cull-Candy, 1992; Fucile et al., 1999; Sukharev et al., 1994). Despite this fact, the five-helix bundle motif in the MscL was proposed as a template for the modeling of LGICs (Chang et al., 1998). Indeed, the aligned sequences of the pore-forming segments of MscL and α_1 GlyR have identical residues $Gly^{2'}$, $Thr^{6'}$ $Thr^{10'}$, $Thr^{13'}$ and $Ser^{15'}$, as well as homologous residues in positions $1'$ $4'$, $8'$, and $9'$ (Table 1). However, the experimental data on the pore-lining residues in nAChR (Akabas et al., 1994) and $GABA_AR$ (Xu and Akabas, 1996) are only partially consistent with the experimental structure of MscL. $Val^{-1'}$, $Gly^{2'}$, $Thr^{6'}$, and, probably, $Val^{9'}$ would be reachable by the ligands from inside the pore of MscL, but $Thr^{13'}$ and $Ile^{16'}$ do not face the pore.

To compare our AChR-based models with MscL, we have built a preliminary homology model of α_1 GlyR using the MscL structure as a template. In the MscL-based homology model, $Thr^{6'}$ residues may donate H-bonds to PTX and to the hydration shell of Cl^- in a manner similar to that found in AChR-based models of GlyRs and GABAR. However, ring $R^{6'}$ in the MscL-based model is essentially larger than in the AChR-based models. The MCM docking of PTX in the MscL-based model of α_1 GlyR yielded a complex with only three H-bonds between PTX and $Thr^{6'}$ residues (Fig. 11) and only three M2s being in a close contact with the ligand. As we discuss below, such a binding mode is energetically less preferable than the ligand binding in a close contact with five M2s.

We further imposed five H-bonding constraints between $Thr^{6'}$ residues and the rounded end of PTX, and allowed M2 helices to translate parallel to the *xy* plane toward the pore axis as rigid bodies while preserving the orientation of the helical axes. An MCM trajectory yielded a low-energy structure more consistent with the AChR-based models in terms of the dimensions of the pore (not shown). Thus, models of LGICs may be

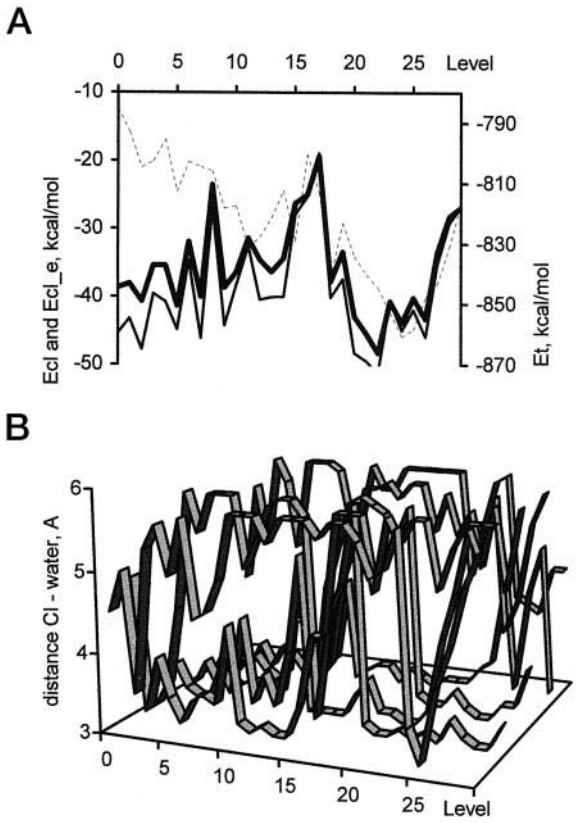

FIGURE 9 (*A*) MC-minimized energy profile of $Cl^-/(H_2O)_8$ in the pore of α_1 GlyR: the total energy of the system (E_t, *dashed line*), the energy of interactions of Cl^- with the receptor and waters (E_{Cl}, *bold line*), and E_{Cl_e} (*thin line*), the electrostatic component of E_{Cl}. (*B*) Distances between Cl^- and water oxygens in the cluster $Cl^-/(H_2O)_8$ against Cl^- position in the pore. Six, two, and four waters closely approach Cl^- at levels 5, 17, and 21, respectively, indicating that Cl^- hydration is affected by the channel micro-architecture. Each water molecule is kept within 6 Å of Cl^- by the flat-bottom constraint Cl^--O with the upper limit of 6 Å.

built by imposing the crossing angles between the pore helices seen in MscL and the dimensions of rings $R^{6'}$ and $R^{2'}$ obtained in the present study. Future systematic analysis should clarify whether such models would explain the pharmacological peculiarities of LGICs.

DISCUSSION

The major aim of the present work is to analyze, using homology modeling and MCM calculations, the possible molecular mechanisms for the block of Cl^- channels by CTB and PTX, and to explain the dependence of their effect on the subunit composition of glycine and GABA receptors.

As described above, CTB and PTX have very different chemical structures. In particular, CTB is an anion expected to bind in the anion-selective pore while PTX is a neutral molecule, and the inhibitory mechanism of this plant alkaloid is still not clear. Experimental results suggest that PTX blocks GABAR- and GlyR-mediated currents in two different ways: 1) as a noncompetitive, channel-blocking antagonist; and 2) as an allosteric antagonist that does not occlude the pore lumen.

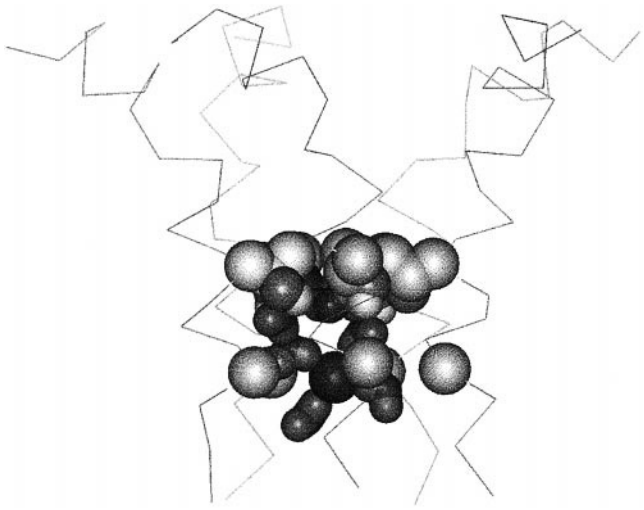

FIGURE 10 MC-minimized complex of the α_1 GlyR with $Cl^-/(H_2O)_8$ at level 23. Receptor, water molecules, and Cl^- are coded by light, medium, and dark shades, respectively.

In favor of the allosteric mechanism are results of whole-cell and single-channel analysis using rat dissociated sympathetic neurons, suggesting that picrotoxin stabilizes an agonist-bound shut state (Newland and Cull-Candy, 1992). This view is also supported by observations on the homomeric α_1 GlyR (Lynch et al., 1995) and $GABA_C$R (Wang et al., 1994; Qian and Dowling, 1994; Zhang et al., 1995a) demonstrating the competitive component of PTX-induced inhibition. This component can be eliminated by mutations of a single amino acid in the M2 segment (Wang et al., 1995).

Several lines of evidence support the noncompetitive, channel-blocking mechanism of PTX action. First, this antagonist inhibits various anion-selective receptor-operated channels independently of the receptor type. Thus, in addition to blocking GABARs and GlyRs, PTX effectively blocks Cl^--dependent currents activated by glutamate (reviewed by Cleland, 1996), acetylcholine (Yarowsky and Carpenter, 1978) or dopamine (Magoski and Bulloch, 1999). Moreover, this alkaloid does not modulate the binding of GABA to its receptor (Enna et al., 1977) and the onset rate of the PTX-induced inhibition of the homomeric GlyR does not depend on the presence of glycine (Lynch et al., 1995). These observations strongly suggest that the site of PTX action does not coincide with the neurotransmitter's recognition sites. Second, site-directed mutations in the pore-facing M2 segment dramatically affect the inhibitory activity of PTX. This was demonstrated on GlyR (Pribilla et al., 1992), homomeric human (Wang at al., 1994, 1995; Enz and Bormann, 1995) and rat (Zhang et al., 1995a) $GABA_C$Rs, and α, β, or γ subunits of $GABA_A$R (Gurley et

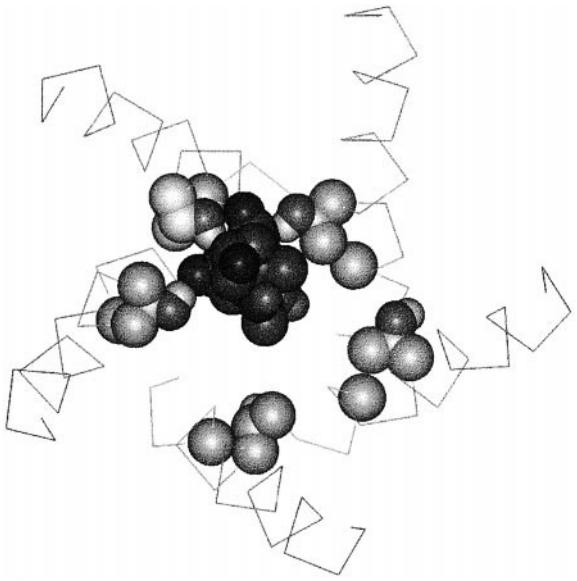

FIGURE 11 Extracellular view of the preliminary homology model of the α_1 GlyR built with the crystallographic structure of the mechanosensitive channel from *Mycobacterium tuberculosis* (Chang et al., 1998) as the template. PTX loosely binds at ring $R^{6'}$, accepting only three H-bonds from $Thr^{6'}$ residues. Receptor and PTX are coded by light and dark shades, respectively.

al., 1995; see Table 2). Third, a synthetic four-helix bundle protein composed of M2 segments from GlyR formed anion-selective channels that were blocked by PTX (Reddy et al., 1993) although the properties of this block were different from those reported for authentic channels (Newland and Cull-Candy, 1992). Fourth, using the substituted-cysteine-accessibility method, Xu et al. (1995) convincingly demonstrated that PTX interacts with the pore-lining residues of the $GABA_AR$ channel. The blocker protected the engineered α_1 $Cys^{2'}$ residue from modification by sulfhydryl reagents. Moreover, in oocytes expressing the mutant with the engineered $Cys^{6'}$ residue, a sulfhydryl reagent, methanethiosulfonate ethylammonium, decreased the PTX-induced block, demonstrating a competition with the blocker for the common binding site comprising $Cys^{6'}$. All these studies clearly indicate that the main target for PTX action is the Cl^--selective pore region.

Although it is possible that receptors can have two distinct types of PTX binding sites (Davis and Ticku, 1981; Yoon et al., 1993), results of our study favor a "pore region" mechanism of PTX action. Assuming that different LGICs share a similar five-helix-bundle architecture of the pore region, we have included in this study homology models of several GlyRs and GABARs, using as a template the model of nAChR in the open state (Tikhonov and Zhorov, 1998). We further performed a systematic search for probable binding sites of two different blockers, CTB and PTX, in the models of Cl^--selective channels.

Mutagenesis experiments suggest that interaction of CTB and PTX with GlyRs and GABARs depend on residues in positions 2′ and 6′ (see Table 2). A simple approach would be to dock the ligands at rings $R^{6'}$ and $R^{2'}$ that have been experimentally demonstrated to affect the ligand binding. However, to avoid a bias, we have performed systematic searches for the energetically most preferable binding sites for CTB and PTX. In each receptor model, a ligand was restrained at 30 levels of the pore, an MCM trajectory was calculated for each level, and parameters of the lowest-energy MECs found in the trajectories were presented as the MC-minimized energy profiles.

General properties of the energy profiles

The MC-minimized energy profiles show the total energy and its major components as a function of the ligand position in the pore. The extracellular half of the pore is wider than either CTB or PTX. At these levels, the ligands may interact with no more than two or three M2s simultaneously, yielding ligand-receptor energy E_{lr} of only ~ -10 kcal/mol (Figs. 4 and 7). The intracellular half of the pore is narrower. A priori, it was not clear whether CTB and PTX would fit there. The fact that all the E_{lr} profiles show large negative values in the intracellular half of the pore indicates that the blockers do fit there and interact with five M2s simultaneously. These interactions may drive the ligand into the narrow pore. Thus, the systematic search revealed that dimensions of both CTB and PTX match cross-sectional dimensions of the inner half of the pore. This is a computational argument in favor of a noncompetitive mechanism of PTX binding.

Because computing an MCM energy profile requires large computational resources, we have not attempted to statistically evaluate a variability of the energy profiles by simulating different runs of the same ligand via the same receptor. An indirect estimate of the variability comes from comparing central stretches of the energy profiles at Fig. 4 *E* that correspond to CTB passing levels 9–20 (M2 positions 10′–3′). At these positions, α_1, α_2, α_1/β, and α_2/β GlyRs have identical or homologous residues (Table 1). At most levels in this area, the ligand-receptor energy of different profiles varies within 5 kcal/mol. In contrast, the ligand receptor energy at levels 5–10 and 21–26 (where M2s have different residues) varies up to 10 kcal/mol.

The minimal values of E_{lr} in the energy profiles (below -30 kcal/mol) are not compatible with the micromolar affinities observed for CTB and PTX in GlyRs and GABARs (Table 2). It should be noted that our calculations take into account only enthalpy contributions to the free energy of ligand-receptor interactions. Free energy calculations that require huge computational resources were not performed in this work (as well as in analogous modeling studies). Thus, the discrepancy between the calculated minimal values of E_{lr} and observed affinities of the blockers is

explained by ignoring in our calculations destabilizing entropy contributions such as ligand and receptor dehydration and the lost of ligand and receptor degrees of freedom in the ligand-receptor complexes.

The profiles of electrostatic energy have deep minima for CTB but not for PTX at the cytoplasmic end of the pore. Since our models represent ionogenic residues in their neutral forms, the minima are due to the macrodipole effect of stabilizing an anion at the N-end of an α-helix (Aqvist et al., 1991; Lockhart and Kim, 1992, 1993; Sitkoff et al., 1994). Macrodipoles from five M2s concertedly stabilize the anionic CTB at the cytoplasmic end of the pore. At first sight, the fact that PTX is not an anion may provide evidence against its binding in the anionic pore. However, the energy profiles for PTX also show a significant contribution of the negative electrostatic energy to the ligand-receptor interactions. Partitioning the ligand-receptor energy shows that interactions of the negatively charged PTX oxygens with the positively charged C′ atoms in the peptide backbone are the major components of the electrostatic stabilization of PTX in the pore.

Another stabilizing factor revealed by our calculations are H-bonds between oxygen atoms at the rounded end of PTX and $Thr^{6'}$ residues. The substitution of $Thr^{6'}$ by Phe in any subunit of the rat $\alpha_1/\beta_2/\gamma_2$ $GABA_AR$ increases IC_{50} for the PTX block by at least two orders of magnitude (Curley et al., 1995; see Table 2). In view of our model, these facts may be explained by the deficiency of H-bond donors in ring $R^{6'}$ of the mutants.

The energy profiles of PTX (Fig. 7 *A*) and hydrated Cl^- (Fig. 9 *A*) in α_1 GlyR have the deepest minima at the same level of the pore, highlighting the analogy in the mechanisms of stabilization of Cl^- and PTX in the Cl^--selective pore. This raises an intriguing question on the possibility of competitive interactions between PTX and Cl^- ions. The "competitive" component of the PTX block reported in several studies (Wang et al., 1994; Qian and Dowling, 1994; Zhang et al., 1995b; Lynch et al., 1995) can be due to this interaction. Indeed, the substantial increase of IC_{50} for a PTX block was observed only at GABA concentrations corresponding to elevation of Cl^- conductance, while the increase of the agonist concentration beyond the saturation point produced only a modest or zero increase in IC_{50} (Wang et al., 1994; Qian and Dowling, 1994). This reveals the necessity of Cl^- channel activation for modulation of the "competitive" component of PTX block. In view of our analysis, this behavior can be explained by the competitive interaction between PTX and Cl^- ions. Moreover, strong reduction of the "competitive" component of the PTX block upon substitution of $Pro^{2'}$ residues by Ser or Gly (Wang et al., 1995) may result from the decrease of this interaction. Further experimental analysis is necessary to test this hypothesis.

Structure-activity relationships in light of the model

Block of ligand-gated Cl^- channels by PTX and PTN

Our models predict that both plant alkaloids, PTX and PTN, would accept H-bonds from $Thr^{6'}$ residues as the elongated end of the blockers enters ring $R^{2'}$. GABARs have hydrophobic residues in ring $R^{2'}$ (Table 2) which would interact with the hydrophobic isopropenyl group of PTX more strongly than with the hydrophilic dimethylmethanol group of PTN. This may explain the low activities of PTN (Jarboe et al., 1968; Curtis and Johnston, 1974) and also α-picrotoxinone (which has an acetyl group in place of the isopropenyl group of PTX) observed with homo-oligomeric *Drosophila melanogaster* RDL GABAR (Shirai et al., 1995). In contrast to their different activities at GABARs, both PTX and PTN block α_1 GlyR with a moderate IC_{50} of ~60 μM (Lynch et al., 1995). Our model explains this observation by the amphipathic nature of the $Gly^{2'}$ ring in the α_1 GlyR. The backbone methylene groups of $Gly^{2'}$ residues would contribute to the hydrophobic interactions with the isopropenyl group of PTX, while water molecules at the backbone C═O and NH groups of $Gly^{2'}$ residues would contribute to hydrophilic interactions with the hydroxyl group at the elongated end of PTN.

Acetylation of the hydroxyl group in PTX yields weakly active picrotoxinin acetate (Shirai et al., 1995). Our model predicts that the PTX hydroxyl forms H-bonds with $Thr^{6'}$ residues, while the blocker passes the $R^{6'}$ ring (Fig. 8 *A*). The substitution of the hydroxyl by the bulkier acetyl group would increase the energy barrier at ring $R^{6'}$. In agreement with this model, the substitution of the PTX hydroxyl by the small fluorine atom has small to moderate effects on the antagonist activity for the insect GABARs (Anthony et al., 1994; Shirai et al., 1995). Anthony et al. (1994) concluded that the activity of the naturally occurring and synthetic PTX-like compounds at insect neuronal GABA-gated Cl^- channels depends on the ability of the bridgehead group to form a hydrogen bond and the lipophilic nature of the terminal isopropenyl group. These observations are also in line with our model that predicts the elongated end of PTX to bind in a hydrophobic ring $R^{2'}$ and the PTX hydroxyl to form an H-bond with the receptor while passing the $R^{6'}$ ring (Fig. 8 *A*).

Xu et al. (1995) demonstrated that the extracellularly applied, negatively charged, sulfhydryl-specific reagent, 4-chloromercuribenzenesulfonate (pCMBS-), irreversibly inhibited the GABA-induced currents in the receptors with engineered $Cys^{2'}$ and $Cys^{6'}$ residues in the α_1 subunit of GABAR, while PTX protected the $Cys^{2'}$ residues from the interaction with pCMBS-. These experiments clearly demonstrate that PTX binds at ring $R^{2'}$, in agreement with our model. Although our calculations cannot rule out competitive components of the PTX action, they show that H-bonds, electrostatic, and van der Waals interactions stabilize PTX

binding in the anion-selective pore. It is difficult to expect a similar network of interactions stabilizing PTX binding in the receptor's recognition sites for the zwitterionic glycine and GABA agonists.

Substitution of $Thr^{6'}$ in GABARs by Met (Zhang et al., 1995a) or Phe (Curley et al., 1995) dramatically affects the sensitivity to PTX. Our model explains this fact by the lack of the H-bonding donors in the side chains of $Met^{6'}$ and $Phe^{6'}$ residues. The model does not explain the observation by Zhang et al. (1995b) that co-expression of *Drosophila melanogaster* RDL and $LCCH_3$ subunits, both of which have $Ala^{2'}$ and $Thr^{6'}$ residues (see Table 1), yields PTX-insensitive receptors. These subunits, however, have essentially different sequences (RNATP and HEATS, respectively) upstream from the position 1′, in the region that may be involved in channel gating (Wilson and Karlin, 1998).

Block of GlyRs by CTB compared with the block of nAChR by triphenylmethylphosphonium

The overall shape of CTB resembles that of triphenylmethylphosphonium ($TPMP^+$), a noncompetitive antagonist that labels the δ $Ser^{6'}$ residue in the resting, desensitized, and closed states of nAChR (Hucho et al., 1986). The accessibility of the $Ser^{6'}$ residue in the closed channel is in agreement with the notion that the activation gates of nAChRs are between positions −1′ and 2′ (Wilson and Karlin, 1998).

In contrast to $TPMP^+$ interactions with ring $R^{6'}$ in nAChR, binding of CTB to GlyRs was strongly affected by mutations in positions 2′ (Table 2). Our model suggests two reasons for this apparent discrepancy. First, the ring of bulky $Thr^{6'}$/$Phe^{6'}$ residues in GlyRs should be narrower than the ring of $Ser^{6'}$ residues in nAChRs. In contrast, the ring of the $Thr^{2'}$ residues in nAChRs should be narrower than the ring of $Gly^{2'}$/$Ala^{2'}$/$Pro^{2'}$ residues in GlyRs. Although the ring of $Thr^{6'}$ residues in GlyRs allows CTB to pass through, it does not constitute a low-energy binding site: note barriers at level 16 in the energy profiles of CTB in GlyRs (Fig. 4). Second, helical macrodipoles stabilize the association of anions, but not cations, at the N-termini of the helices. Therefore, the macrodipoles would favor interaction of the anionic CTB at ring $R^{2'}$, as indicated by the deep minimum of the electrostatic interactions of CTB at ring $R^{2'}$ (Fig. 4). In contrast, the macrodipole effect would disfavor association of the cationic $TPMP^+$ at ring $R^{2'}$. Thus, both steric and electrostatic effects concertedly stabilize binding of $TPMP^+$ at ring $R^{6'}$ of nAChR and binding of CTB at the ring $R^{2'}$ of GlyRs.

Dimensions of the pore

The size of LGICs is usually described in terms of the dimensions of the largest permeating organic ions approximated by simple geometrical figures, such as squares (Dwyer et al., 1980), circles (Bormann et al., 1987; Nutter and Adams, 1995), or rectangles (Zhorov et al., 1991). The permeating organic cations have minimal silhouettes that do not exactly match the simple geometrical figures. The snapshots of the large star-like CTB passing the ring of $Thr^{6'}$/$Phe^{6'}$ residues (Fig. 6) clearly show that it is not possible to represent a silhouette of a pore by any simple geometrical figure. Our results demonstrate that PTX and CTB may bind at the narrow levels of Cl^- channels. The fact that PTX blocks a synthetic four-helix-bundle Cl^--selective channel (Reddy et al., 1993) is also consistent with our model of PTX binding in a narrow Cl^--selective pore.

Horenstein and Akabas (1998) demonstrated that μM concentrations of Zn^{2+} block an engineered $GABA_AR$ with five $His^{17'}$ residues, suggesting that the Zn^{2+} binding site involves His-17′ residues from at least two subunits and that 17′ C^α atoms are separated by <13 Å. In our model, 17′ C^α atoms in the neighboring M2s are separated by 15–17 Å. At this stage, it is difficult to conclude whether the inconsistency of the model with the experiment is due to an incorrectness of the model, mobility of M2s in real $GABA_AR$, or other reasons. In any case, 17′ residues are at the widest part of the pore and are not involved in the binding of PTN and CTB.

CONCLUSIONS

In this work we have built models of the pore region in glycine and GABA receptors using as a template the model of nAChR by Tikhonov and Zhorov (1998). In the absence of a high-resolution structure of LGICs, the correctness of the template is unknown. This fact naturally concerns the homology models. However, the latter explained experimental observations that have not been used to create the template. Among these observations are the channel-blocking effects of CTB, PTX, and PTX analogs, as well as intriguing paradoxes in the relationships between the subunit composition of Cl^- channels and their sensibility to the blockers. This evidence supports the general pore architecture of LGICs proposed in this and the earlier studies. The models suggest that the binding of PTX and CTB in the cytoplasmic half of the pore is stabilized by van der Waals interactions with five M2 segments. Helical macrodipoles contribute to the anionic selectivity of Cl^- channels and stabilize CTB binding in GlyRs, while the binding of PTX is stabilized by H-bonds donated by $Thr^{6'}$ residues. The models also suggest that the resistance of α_2 GlyR to the PTX block is due to a lack of room between $Ala^{2'}$ and $Thr^{6'}$ rings, while the resistance of α_1/β GlyR and mutants of GABARs to the PTX block is due to lack of H-bond donors on the side chains of $Phe^{6'}$ or $Met^{6'}$ residues. The predicted dimensions of $R^{6'}$ and $R^{2'}$ rings in glycine and GABA receptors suggest a narrow cytoplasmic half of the pore, in agreement with various pharmacological, electrophysiological, and mutagenesis experiments. These dimensions may be used as constraints for further homology modeling of

LGICs that take into account the folding of the pore-forming α-helices observed in the crystallographic structure of the mechanosensitive channel.

We thank Stuart Edelstein and Richard Epand for critical reading of the manuscript, Henry Korn for his interest in this work, and Ekaterina Folkman for assistance with figure preparation. B.S.Z. acknowledges a Visiting Professor award from the French Ministry of Education, Science, and Technology, and partial support from the Russian Foundation for Basic Research (Grant 99-04-49815).

REFERENCES

Abagyan, R., and M. Totrov. 1994. Biased probability Monte Carlo conformational searches and electrostatic calculations for peptides and proteins. *J. Mol. Biol.* 235:983–1002.

Adcock, C., G. R. Smith, and M. S. Sansom. 1998. Electrostatics and the ion selectivity of ligand-gated channels. *Biophys. J.* 75:1211–1222.

Akabas, M. H., and A. Karlin. 1995. Identification of acetylcholine receptor channel-lining residues in the M1 segment of the α-subunit. *Biochemistry.* 34:12496–12500.

Akabas, M. H., C. Kaufmann, P. Archdeacon, and A. Karlin. 1994. Identification of acetylcholine receptor channel-lining residues in the entire M2 segment of the alpha subunit. *Neuron.* 13:919–927.

Anthony, N. M., C. W. Holyoke, Jr., and D. B. Sattelle. 1994. Blocking actions of picrotoxinin analogues on insect (Periplaneta americana) GABA receptors. *Neurosci. Lett.* 171:67–69.

Aqvist, J., H. Luecke, F. A. Quiocho, and A. Warshel. 1991. Dipoles localized at helix termini of proteins stabilize charges. *Proc. Natl. Acad. Sci. U.S.A.* 88:2026–2030.

Arias, H. R. 1998. Binding sites for exogenous and endogenous noncompetitive inhibitors of the nicotinic acetylcholine receptor. *Biochim. Biophys. Acta.* 1376:173–220.

Betz, H. 1990. Ligand-gated ion channels in the brain: the amino acid receptor subfamily. *Neuron.* 5:383–392.

Bormann, J., O. P. Hamill, and B. Sakmann. 1987. Mechanism of anion permeation through channels gated by glycine and γ-aminobutyric acid in mouse cultured spinal neurones. *J. Physiol.* 385:243–286.

Brooks, C. L., B. M. Pettitt, and M. Karplus. 1985. Structural and energetic effects of truncating long ranged interactions in ionic polar fluids. *J. Chem. Phys.* 83:5897–5908.

Brovtsyna, N. B., D. B. Tikhonov, O. B. Gorbunova, V. E. Gmiro, S. E. Serduk, N. Ya. Lukomskaya, L. G. Magazanik, and B. S. Zhorov. 1996. Architecture of the neuronal nicotinic acetylcholine receptor ion channel at the binding site of bis-ammonium blockers. *J. Membr. Biol.* 152: 77–87.

Chang, G., R. H. Spencer, A. T. Lee, M. T. Barclay, and D. C. Rees. 1998. Structure of the MscL homolog from Mycobacterium tuberculosis: a gated mechanosensitive ion channel. *Science.* 282:2220–2226.

Changeux, J. P., J. L. Galzi, A. Devillers-Thiery, and D. Bertrand. 1992. The functional architecture of the acetylcholine nicotinic receptor explored by affinity labeling and site-directed mutagenesis. *Q. Rev. Biophys.* 25:395–432.

Cleland, T. A. 1996. Inhibitory glutamate receptor channels. *Mol. Neurobiol.* 13:97–136.

Curley, D., J. Amin, P. C. Ross, D. S. Wess, and G. White. 1995. Point mutations in the M2 region of the alpha, beta, or gamma subunit of the $GABA_A$ channel that abolish block by picrotoxin. *Receptors and Channels.* 3:13–20.

Curtis, D. R., and G. A. R. Johnston. 1974. Neuropoisons: Their Pathophysiological Actions. Vol. 2. Poisons of Plant Origin. L. L. Simpson and D. R. Curtis, editors. Plenum Press, New York.

Davis, W. C., and M. K. Ticku. 1981. Picrotoxinin and diazepam bind to two distinct proteins: further evidence that pentobarbital may act at the picrotoxinin site. *J. Neurosci.* 1:1036–1042.

Doyle, D. A., J. M. Cabral, R. A. Pfuetzner, A. Kuo, J. M. Gulbis, S. L. Cohen, B. T. Chait, and R. MacKinnon. 1998. The structure of the potassium channel: molecular basis of K^+ conduction and selectivity. *Science.* 280:69–77.

Dwyer, T. M., D. J. Adams, and B. Hille. 1980. The permeability of the endplate channel to organic cations in frog muscle. *J. Gen. Physiol.* 75:469–492.

Enna, S. J., J. F. Collins, and S. H. Snyder. 1977. Stereospecificity and structure-activity requirements of GABA receptor binding in rat brain. *Brain Res.* 124:185–190.

Enz, R., and J. Bormann. 1995. A single point mutation decreases picrotoxinin sensitivity of the human GABA receptor rho 1 subunit. *Neuroreport.* 6:1569–1572.

Fucile, S., D. de Saint Jan, B. David-Watine, H. Korn, and P. Bregestovski. 1999. Comparison of glycine and GABA actions on the zebrafish homomeric glycine receptor. *J. Physiol. (Lond.).* 517:369–383.

Galzi, J. L., and J. P. Changeux. 1995. Neuronal nicotinic receptors: molecular organisation and regulations. *Neuropharmacology.* 34: 563–582.

Galzi, J. L., A. Devillers-Thiery, N. Hussy, S. Bertrand, J.-P. Changeux, and D. Bertrand. 1992. Mutations in the channel domain of a neuronal nicotinic receptor convert ion selectivity from cationic to anionic. *Nature.* 359:500–505.

Gurley, D., J. Amin, P. C. Ross, D. S. Weiss, and G. White. 1995. Point mutations in the M2 region of the α, β, or γ subunit of the $GABA_A$ channel that abolish block by picrotoxin. *Receptors and Channels.* 3:13–20.

Horenstein, J., and M. H. Akabas. 1998. Location of a high affinity Zn^{2+} binding site in the channel of α_1 β_1 γ-aminobutyric $acid_A$ receptors. *Mol. Pharmacol.* 53:870–877.

Hosie, A. M., K. Aronstein, D. B. Sattelle, and R. H. ffrench-Constant. 1997. Molecular biology of insect neuronal GABA receptors. *Trends Neurosci.* 20:578–583.

Hucho, F., W. Oberthur, and F. Lottspeich. 1986. The ion channel of the nicotinic acetylcholine receptor is formed by the homologous helices M II of the receptor subunits. *FEBS Lett.* 205:137–142.

Imoto, K., C. Busch, B. Sakmann, M. Mishina, T. Konno, J. Nakai, H. Bujo, Y. Mori, K. Fukuda, and S. Numa. 1988. Rings of negatively charged amino acids determine the acetylcholine receptor channel conductance. *Nature.* 335:645–648.

Jarboe, C. H., L. A. Poerter, and R. T. Buckler. 1968. Structural aspects of picrotoxinin action. *J. Med. Chem.* 11:729–731.

Karlin, A., and M. H. Akabas. 1995. Toward a structural basis for the function of nicotinic acetylcholine receptors and their cousins. *Neuron.* 15:1231–1244.

Labarca, C., M. W. Nowak, H. Zhang, L. Tang, P. Deshpande, and H. A. Lester. 1995. Channel gating governed symmetrically by conserved leucine residues in the M2 domain of nicotinic receptors. *Nature.* 376: 514–516.

Langosch, D., L. Thomas, and H. Betz. 1988. Conserved quaternary structure of ligand-gated ion channels: the postsynaptic glycine receptor is a pentamer. *Proc. Natl. Acad. Sci. U.S.A.* 185:7394–7398.

Lester, H. A. 1992. The permeation pathway of neurotransmitter-gated ion channels. *Annu. Rev. Biophys. Biomol. Struct.* 21:267–292.

Li, Z., and H. A. Scheraga. 1988. Structure and free energy of complex thermodynamic systems. *J. Mol. Struct. (THEOCHEM).* 179:333–352.

Lockhart, D. J., and P. S. Kim. 1992. Internal stark effect measurement of the electric field at the amino terminus of an α helix. *Science.* 257: 947–951.

Lockhart, D. J., and P. S. Kim. 1993. Electrostatic screening of charge and dipole interactions with the helix backbone. *Science.* 260:198–202.

Lynch, J. W., S. Rajendra, P. H. Barry, and P. R. Schofield. 1995. Mutations affecting the glycine receptor agonist transduction mechanism convert the competitive antagonist, picrotoxin, into an allosteric potentiator. *J. Biol. Chem.* 270:13799–13806.

Magoski, N. S., and A. G. Bulloch 1999. Dopamine activates two different receptors to produce variability in sign at an identified synapse. *J. Neurophysiol.* 81:1330–1340.

Momany, F. A., R. F. McGuire, A. W. Burgess, and H. A. Scheraga. 1975. Energy parameters in polypeptides. VII. Geometric parameters, partial atomic charges, nonbonded interactions, hydrogen bond interactions, and intrinsic torsional potentials of the naturally occurring amino acids. *J. Phys. Chem.* 79:2361–2381.

Newland, C. F., and Cull-Candy, S. G. 1992. On the mechanism of action of picrotoxin on GABA receptor channels in dissociated sympathetic neurones of the rat. *J. Physiol. (Lond.).* 447:191–213.

Nutter, T. J., and D. J. Adams. 1995. Monovalent and divalent cation permeability and block of neuronal nicotinic receptor channels in rat parasympathetic ganglia. *J. Gen. Physiol.* 105:701–723.

Ortells, M. O., and G. G. Lunt. 1995. Evolutionary history of the ligand-gated ion-channel superfamily of receptors. *Trends Neurosci.* 18: 121–127.

Ortells, M. O., and G. G. Lunt. 1996. A mixed helix-β-sheet model of the transmembrane region of the nicotinic acetylcholine receptor. *Protein Eng.* 9:51–59.

Pribilla, I., T. Takagi, D. Langosch, J. Bormann, and H. Betz. 1992. The atypical M2 segment of the β subunit confers picrotoxinin resistance to inhibitory glycine receptor channels. *EMBO J.* 11:4305–4311.

Qian, H., and J. E. Dowling. 1994. Pharmacology of novel GABA receptors found on rod horizontal cells of the white perch retina. *J. Neurosci.* 14:4299–4307.

Reddy, G. L., T. Iwamoto, J. M. Tomich, and M. Montal. 1993. Synthetic peptides and four-helix bundle proteins as model systems for the pore-forming structure of channel proteins. II. Transmembrane segment M2 of the brain glycine receptor is a plausible candidate for the pore-lining structure. *J. Biol. Chem.* 268:14608–14615.

Revah, F., D. Bertrand, J. L. Galzi, A. Devillers-Thiery, C. Mulle, N. Hussy, S. Bertrand, M. Ballivet, and J. P. Changeux. 1991. Mutations in the channel domain alter desensitization of a neuronal nicotinic receptor. *Nature.* 353:846–849.

Rundström, N., V. Schmieden, H. Betz, J. Bormann, and D. Langosch. 1994. Cyanotriphenylborate: subtype-specific blocker of glycine receptor chloride channels. *Proc. Natl. Acad. Sci. U.S.A.* 91:8950–8954.

Sankararamakrishnan, R., C. Adcock, and M. S. P. Sansom. 1996. The pore domain of the nicotinic acetylcholine receptor: molecular modeling, pore dimensions, and electrostatics. *Biophys. J.* 71:1659–1671.

Shirai, Y., A. M. Hosie, S. D. Buckingham, C. W. Holyoke, Jr., H. A. Baylis, and D. B. Sattelle. 1995. Actions of picrotoxinin analogues on an expressed, homo-oligomeric GABA receptor of Drosophila melanogaster. *Neurosci. Lett.* 189:1–4.

Sitkoff, D., D. J. Lockhart, K. A. Sharp, and B. Honig. 1994. Calculation of electrostatic effects at the amino terminus of an α helix. *Biophys. J.* 67:2251–2260.

Sukharev, S. I., P. Blount, B. Martinac, F. R. Blattner, and C. Kung. 1994. A large-conductance mechanosensitive channel in *E. coli* encoded by MscL alone. *Nature.* 368:265–268.

Tikhonov, D. B., and B. S. Zhorov. 1998. Kinked-helices model of the nicotinic acetylcholine receptor ion channel and its complexes with blockers: simulation by the Monte Carlo minimization method. *Biophys. J.* 74:242–255.

Unwin, N. 1995. Acetylcholine receptor channel imaged in the open state. *Nature.* 73:37–43.

Wang, T. L., W. B. Guggino, and G. R. Cutting. 1994. A novel γ-aminobutyric acid receptor subunit (rho 2) cloned from human retina forms bicuculline-insensitive homooligomeric receptors in *Xenopus* oocytes. *J. Neurosci.* 14:6524–6531.

Wang, T. L., A. S. Hackam, W. B. Guggino, and G. R. Cutting. 1995. A single amino acid in γ-aminobutyric acid rho 1 receptors affects competitive and noncompetitive components of picrotoxin inhibition. *Proc. Natl. Acad. Sci. U.S.A.* 92:11751–11755.

Weiner, S. J., P. A. Kollman, D. A. Case, U. C. Singh, C. Chio, G. Alagona, S. Profeta, and P. K. Weiner. 1984. A new force field for molecular mechanical simulation of nucleic acids and proteins. *J. Am. Chem. Soc.* 106:765–784.

Wilson, G. G., and A. Karlin. 1998. The location of the gate in the acetylcholine receptor channel. *Neuron.* 20:1269–1281.

Xu, M., and M. H. Akabas. 1996. Identification of channel-lining residues in the M2 membrane-spanning segment of the $GABA_A$ receptor α_1 subunit. *J. Gen. Physiol.* 107:195–205.

Xu, M., D. F. Covey, and M. H. Akabas. 1995. Interaction of picrotoxin with $GABA_A$ receptor channel-lining residues probed in cysteine mutants. *Biophys. J.* 69:1858–1867.

Yang, J. 1990. Ion permeation through 5-hydroxytryptamine-gated channels in neuroblastoma N18 cells. *J. Gen. Physiol.* 96:1177–1198.

Yarowsky, J., and D. O. Carpenter. 1978. A comparison of similar ionic responses to γ-aminobutyric acid and acetylcholine. *J. Neurophysiol.* 41:531–541.

Yoon, K. W., D. F. Covey, and S. M. Rothman. 1993. Multiple mechanisms of picrotoxin block of GABA-induced currents in rat hippocampal neurons. *J. Physiol. (Lond.).* 464:423–439.

Zhang, H. G., H. J. Lee, T. Rocheleau, R. H. ffrench-Constant, and M. B. Jackson. 1995b. Subunit composition determines picrotoxin and bicuculline sensitivity of Drosophila γ-aminobutyric acid receptors. *Mol. Pharmacol.* 48:835–840.

Zhang, D., Z. H. Pan, X. Zhang, A. D. Brideau, and S. A. Lipton. 1995a. Cloning of a γ-aminobutyric acid type C receptor subunit in rat retina with a methionine residue critical for picrotoxinin channel block. *Proc. Natl. Acad. Sci. USA.* 92:11756–11760.

Zhorov, B. S. 1981. Vector method for calculating derivatives of energy of atom-atom interactions of complex molecules according to generalized coordinates. *J. Struct. Chem.* 22:4–8.

Zhorov, B. S., and V. S. Ananthanarayanan. 1993. Conformational analysis of free and Ca(2+)-bound forms of verapamil and methoxyverapamil. *J. Biomol. Struct. Dyn.* 11:529–540.

Zhorov, B. S., and V. S. Ananthanarayanan. 1996. Structural model of synthetic Ca^{2+} channel with bound Ca^{2+} ions and dihydropyridine ligand. *Biophys. J.* 70:22–37.

Zhorov, B. S., N. B. Brovtsyna, V. E. Gmiro, N. Ya. Lukomskaya, S. E. Serduk, N. N. Potapyeva, L. G. Magazanik, D. E. Kurenniy, and V. I. Skok. 1991. Dimensions of the ion channel in neuronal nicotinic acetylcholine receptor as estimated from analysis of conformation-activity relationships of open-channel blocking drug. *J. Membr. Biol.* 121: 119–132.

Zimmerman, S. S., M. S. Pottle, G. Nemethy, and H. A. Scheraga. 1977. Conformational analysis of the 20 naturally occurring amino acid residues using ECEPP. *Macromolecules.* 10:1–9.